12-2015

Influence of Shelling Temperature and Time on the Optical and Structural Properties of CuInS2/ZnS Quantum Dots

Colette Robinson
University of Arkansas, Fayetteville

Influence of Shelling Temperature and Time on the Optical and Structural Properties of $CuInS_2$/ZnS Quantum Dots

A thesis submitted in partial fulfillment
of the requirements for the degree of
Masters of Science in Chemistry

By

Colette Robinson
Kansas State University
Bachelors of Science in Chemistry, 2012
Kansas State University
Bachelors of Science in Biochemistry, 2012

December 2015
University of Arkansas

This thesis is approved for recommendation to the Graduate Council

_____
Dr. Colin Heyes
Thesis Director

_____
Dr. Bill Durham
Committee Member

_____
Dr. Jingyi Chen
Committee Member

ABSTRACT

CIS/ZnS core/shell QDs are an important class of nanomaterials for optoelectronic, photovoltaic and photoluminescence applications. They consist of lower toxicity materials than the prototypical II-VI Cd-based QDs and show long fluorescence lifetimes, which generates prospective in biological imaging applications. It is vital to develop reproducible synthetic methods for this new class of nanomaterials in order to maintain small sizes with high QYs. CIS core QDs have been shelled with ZnS at various temperatures from 90-210°C for reaction times ranging from 20-140 minutes to examine the role of thermodynamics and kinetics on the shell growth. Using HR-TEM and ICP-MS, it was observed that, rather than growing a ZnS shell onto the cores (as observed for II-VI QDs), ion-exchange occurs, leading to negligible size change at temperatures up to 210°C. Adding Zn via this ion-exchange mechanism leads to an increase in their QY, primarily by increasing the average radiative time through removing surface defects during the exchange process. The Zn concentration and QY is maintained if the shelling temperature is 210°C, but if the temperature is 190°C or lower, Zn is removed over 1-2 hours, although QY is maintained.

After a second injection of the ZnS shelling precursors, both the temperature and time of the reaction have a significant effect on the QY and structural properties. At 210°C, the second injection leads to a significant decrease in the QY, although the Zn concentration is maintained. On the other hand, if the temperature is 190°C or lower, the second injection does not lead to a decrease in the QY. In fact, with time, it can lead to an even higher QY than a single injection at 210°C, even though the Zn concentration drops to almost zero.

Recent reports of CIS/ZnS synthesis have varied within the 190-210°C range. The results in this thesis show that differences in the kinetics of the ion-exchange reactions, alloying between the core and shell, lattice self-purification of CIS and restructuring of the surface between 190°C and 210°C all play crucial roles, and may explain the differences reported in CIS/ZnS optical and structural properties in the literature.

ACKNOWLEDGEMENTS

There have been many people that have been extremely crucial to my well being and development as a student and as a chemist. I would first off like to thank my advisor Dr. Colin Heyes. His unwavering patience and forgiveness was needed more than I can image and most appreciated. He always made sure I came to my own conclusions from possible theories, no matter how upset and frustrated I got with him. I am further grateful that he always took the time to make sure I was still enjoying my research, when I became the most discouraged. He went above and beyond in helping me figure out the next step in my education.

I would also to thank Dr. Bill Durham and Dr. Jingyi Chen for serving on my committee and their patience with my last minute meeting schedules and rescheduling. I would like to extend this thankfulness to Dr. Mourad Benamara for the countless hours he spent collecting TEM images with me and Dr. Erik Pollock who helped me with the elemental composition studies. A special thanks go out to my lab mates, especially our previous post-doc Dr. Gopa Mandal, who taught me how to make CIS QDs and really helped get this project started. Others lab mates and colleagues that deserve my gratitude are the now Dr. Ashley Howard, Randee McBride and Lucas Whisenhunt, for their friendships and always being there to encourage me on a hard day. I am also most appreciative of Dr. Chris Mazzanti, who has been extremely crucial in my development as a better student and teaching assistant. He has always had advice to help me understand theories and how to deal with the wide array of students' emotions that occur with grades and safety.

I would like to extend my upmost thanks and gratitude to all of my parents, Coleen, Dan, Steve, and Shelly. They have never had an inkling about the chemistry or graduate school problems that I have encountered over the last few years but they have always listened intently and offered advice as they could. When I experienced educational setbacks and doubted my abilities the most, they were always there encouraging and reassuring me. I could not be more grateful for their pride in me over the years; it reassures me that no matter what I end up doing I have come a long way from that little curious eight year who loved all things science. Lastly, I would like to thank anyone who has helped me on this project and supported me in this expedition that I have forgotten to mention.

DEDICATION

I would like to dedicate this thesis to Emmanuel Tamayo, my significant other of more than 6 years. Your love, support, patience, forgiveness, and help have not gone unappreciated. The sacrifices you have made for our relationship in order for me to follow my dreams and achieve my professional goals have helped me the most in this journey. I cannot thank you enough or find the words to show how much gratitude that I hold for all your kind actions and supportive words. Thank you.

TABLE OF CONTENTS

Chapter 1: Introduction

1.1 Quantum Dots

The general definition of a quantum dot (QD) is a material in which the charge carriers are confined in all three dimensions, which leads to size dependent properties. In this thesis, we will refer more specifically to a QD as a colloidal semiconductor nanocrystal between 2 and 10 nm in diameter. In this range, the semiconductor nanocrystal is smaller in size than the Bohr radius of its exciton, leading to quantum confinement effects, which determines the absorption and photoluminescence energy; the smaller the nanocrystal is, the larger the band gap energy (**Figure 1.1).**

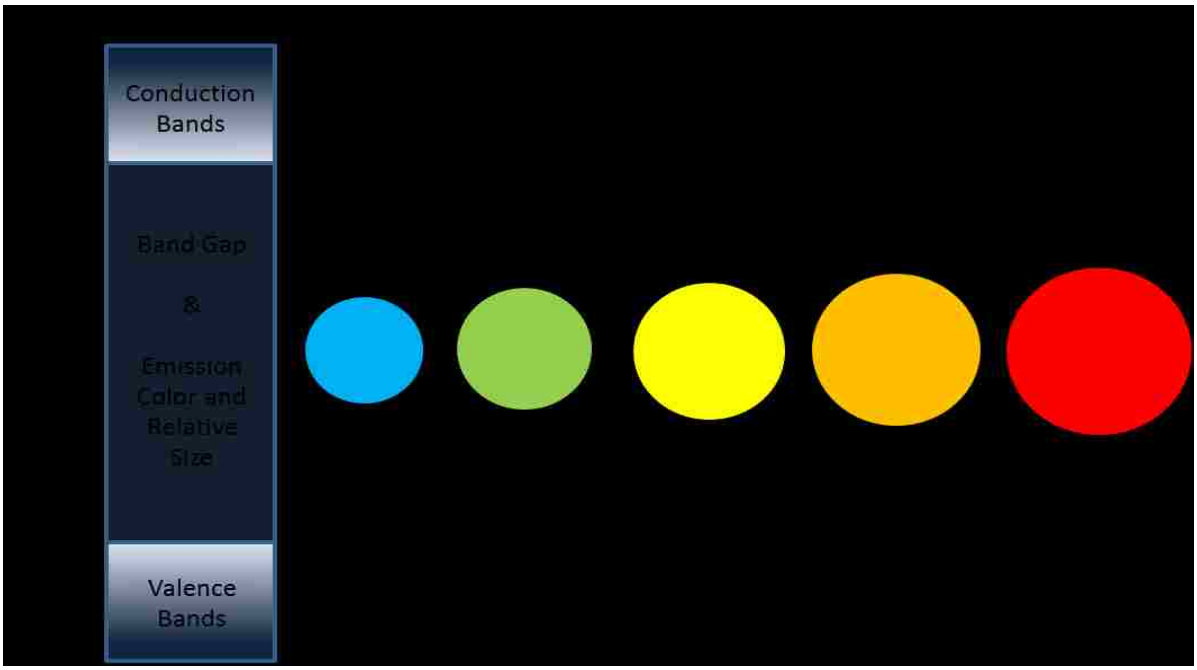

Figure 1.1. The relationship between the band gap and the QD size and color.

The quantum confinement is not only affected by the size of the quantum dot but can also be tuned by varying the material composition of the quantum dots, which changes the Bohr exciton radius.[1] The material of which quantum dots are comprised determine the crystal lattice structure. When a shell is added, the added material can cause the lattice structure to be distorted, called lattice mismatch. Electron or hole trap states can arise from the lattice mismatch at core-shell interfaces or due to incomplete surface passivation at the QD-ligand interface. When an electron is excited to the conduction band,

leaving behind a hole in the valence band, the resulting delocalization exciton can either recombine radiatively, emitting a photon, or one (or both) of the charge carriers can become localized (trapped) in the various trap states. The donor-acceptor pair, DAP,[2] may have different recombination dynamics than the delocalized exciton. If the trapped electron is recombined with the trapped hole, it can also cause luminescence, but the energy from the trapped charge carrier(s) may also be released via non-radiative routes.[3]

The intensity of the luminescence is used to determine the QY, when compared to a known fluorophore. The equation for fluorescence QY, Φ, is:

$$\Phi = \frac{\#\ of\ photons\ emitted}{\#of\ photons\ absorbed} \qquad \textbf{Eqn. 1}$$

The length of time elapsed between the photon absorption and the photon emission is known as the fluorescence lifetime or, more generally, the photoluminescence (PL). Longer lifetimes can be helpful in biological imaging applications because, if the fluorophore has a longer lifetime than the biological media being imaged, time gated imaging (TGI) can be utilized, which delays the detection time relative to the exciting photon pulse. This allows the "noise" or background fluorescence from the biological media to be removed from the image. The fluorescence lifetime, along with QY, can also be used to calculate the radiative and non-radiative rates, which provide information about the physical mechanism(s) by which the fluorescence occurs. The equations for these calculations are (k: rate, τ: lifetime, fl: fluorescence, r: radiative, nr: non-radiative)[4];

$$k_r = \left(\frac{QY}{\tau_{fl}}\right) \qquad \textbf{Eqn. 2}$$

$$k_{nr} = \left(\frac{1}{\tau_{fl}}\right) - k_r \qquad \textbf{Eqn. 3}$$

It is known that QDs viewed at the single molecule level exhibit fluorescence intermittency, also known as blinking. Although the exact mechanism is still not fully understood, two general explanations have been proposed: electron (or hole) trap states (donor-acceptor pair (DAP)) or non-radiative Auger-recombination.[2] DAP occurs when the electron (donor) is recombined with the acceptor (trap state), in which this energy can sometimes be given off as heat (non-radiatively) instead of luminescence (radiatively). Non-radiative Auger recombination occurs when the energy from an exciton is transferred to

an extra charge carrier, which can be an electron for a negatively charged QD or a hole for a positively charged QD.[5] Copper Indium Sulfide/Zinc Sulfide (CIS/ZnS) QDs are an example of Type I QDs[6], where both the electron and hole pair are confined in the core,[7] leading to the size of the QD having a minimal effect on the radiative lifetime,[8] in contrast to Type II QDs, where the electron and hole are charge-separated into the core and shell.

1.2 Copper Indium Sulfide QDs as an alternative to Cd-based QDs

It has long been known that cadmium is carcinogenic and toxic. Studies on Cd-based QDs in rats have shown a decrease in motor function and the onset of necrosis over an extended period of time.[9] Toxic and detrimental effects were observed at concentrations above 1 μM, with minor toxicity effects at concentrations below 1 μM.[9] A recent study by Chen, et al, on the cytotoxicity of CIS and CIS/ZnS QDs, in HeLa and $OECM^{-1}$ cells showed that, after 72 hours of incubation, over 90% of the cells were still viable.[10] Another cytotoxicity study of CIS/ZnS using human macrophages supplemented with 10% fetal bovine serum showed over 90% cell viability after 48 hours even with concentrations of 300 μg mL^{-1}, which is a much higher concentration than used in the Cd-based QD studies.[6]

One optical property that CIS has advantage over Cd-based QDs is the photoluminescence (PL) range that it is tunable over; 500 nm to the near-infrared region of 900 nm, [6,11,12] with the full width at half maximum (FWHM) ranging between 90-150 nm.[6,12,13] Cd based QDs have a tunable range of 450 to 650 nm[1,14], a range in which biological autofluorescence is more problematic, although the FWHM is a much smaller value of 13-35 nm, [12, 14] and are thus more suitable for multicolor imaging. The PL lifetimes show a stark contrast between the CIS and Cd-based QDs. CIS QDs have PL lifetimes ranging between 100 and 300 ns[12,13] and PL lifetimes of Cd-based QDs typically range between 10 and 30 ns.[12] The longer lifetimes of CIS make them more optimal for use in the method of time-gated imaging, an advanced technique used in bioimaging. CIS also have larger Stokes shifts ranging from 100-300 meV,[12] whereas Cd based QDs have Stokes shifts less than ~50 meV.[12] Having a larger Stokes shift reduces the possibility of the QDs re-absorbing their emitted photons, thus reducing inner-filter effects. The QYs of CIS and Cd-based QDs are quite comparable, with CIS being slightly lower, but the other advantageous optical properties balance this lower QY.

Another major advantage of the CIS QDs is their size. The average size of CIS and CIS/ZnS QDs is between 2 and 5 nm,[11, 13, 15, 16] whereas CdSe/ZnS usually vary from 8 to 13 nm[17, 18] depending on their shell thickness. CdSe QDs require thick shells due to the fact that they can be strongly quenched by the coordinating ligands used in aqueous environments.[19] The lower size of CIS makes them ideal for many biological applications. The small size renders them less intrusive for labeling proteins and more capable of entering cells through small channels, so they become more bio-available than Cd-based QDs.

1.3 Optimization of QDs

There are many ways that QDs can be optimized or tuned to meet specific requirements that are desired by certain applications. The major methods of tuning PL properties are; size tuning, composition tuning, and surface tuning; schematics of which are shown in **Figure 1.2**.[12]

Size tuning is the most widely known and exploited and is discussed above in terms of quantum confinement; in **Figure 1.1**, as the size of the QD size increases the band gap decreases making the wavelength longer. It is known that the band gaps are size dependent, so the longer that QDs are left to grow, the lower their band gap and longer the PL emission wavelength become.

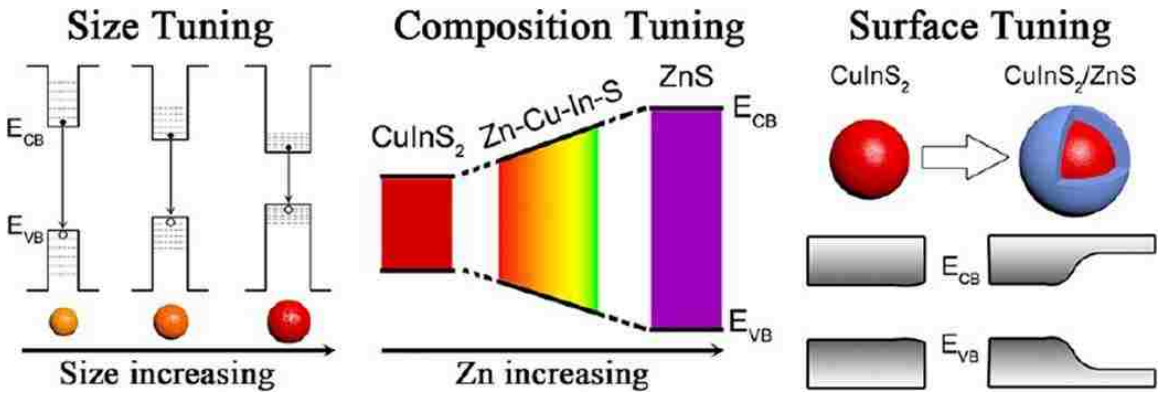

Figure 1.2. Schematic diagrams of the different optimization methods. From Zhong, H., et al., *J. Phys. Chem. Lett.*, 2012, 3, 3167-3175.[12]

Composition tuning is accomplished by varying the composition ratios of the elements involved or by alloying the core and the shell materials together. Varying the composition ratios is quite a common approach and effective at changing the band gap.[12, 20, 21] Changing the element composition ratio

changes the band gap due to changing the atomic packing within the crystal. Different crystal arrangements will have differing emission centers. Different emission center locations and their relative density can lead to changes in the λ_{max}, QY, and FWHM of the QD. Finding the optimal composition for specific emission wavelengths can lead to a QD that is tunable, while still maintaining a high QY, which is currently a major goal of nanoparticle research. Only a few composition ratio studies have been reported so far on CIS QDs.[6, 11]

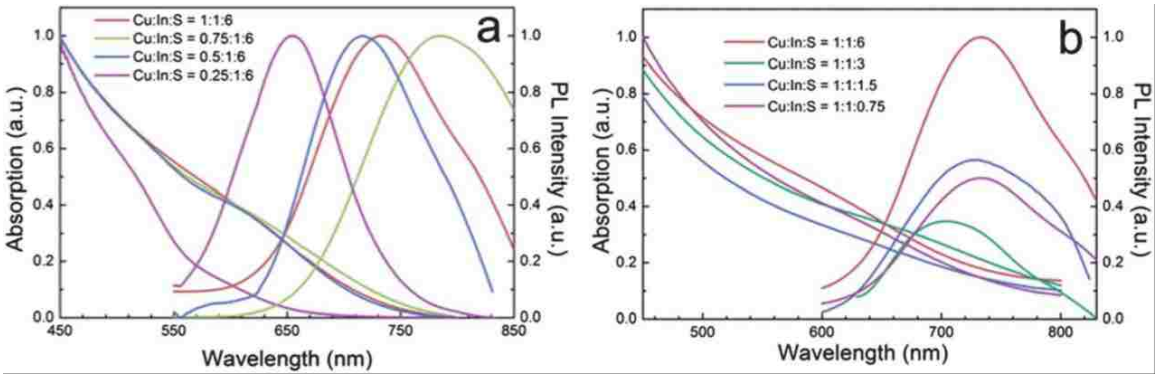

Figure 1.3. Show how different elements have different effects when varying the material composition. From Liu, L., et al., *Analyst*, 2013, 138, 6144-6153.[6]

Figure 1.3, **A** shows how varying the Cu ion concentration while maintaining the In to S ratio affects the absorption spectrum. As the Cu ratio decreases, there is first a red-shift then a blue-shift that occurs. This shows that different composition ratios have a significant impact on the optical and structural properties of CIS. Part B of **Figure 1.3**, shows the result of varying the S ratio with respect to Cu and In. There is only a very slight blue-shift with decreasing sulfur composition. However there is a significant change in the PL intensity (or QY) with the varying ratios. A ratio of 1:1:6 Cu:In:S gives the highest luminescence, which is likely due to increasing the number of sulfur atoms at the QD surface leading to better surface passivation. The sulfur groups on the ligands cause the electron density to be redistributed, increasing the confinement energy resulting in a blue-shift in the λ_{max}, decreasing the number of available trap states thus leading to higher QYs.[22] The second example just varies the Cu:In ratio, which is shown in **Figure 1.4**. When the In concentration is higher than Cu the QY tends to be quite high, being optimal at ratios of Cu:In of 0.4-0.7. A slow blue-shift is also observed, so varying the Cu:In ratio allows for size tuning[23] as

well as QY tuning. When the Cu concentration is higher than In, the PL intensity decreases, reaching zero at a ratio of 2.5:1 or above. This could mean that many trap states or defects are formed when too much Cu is present at the QD surface.

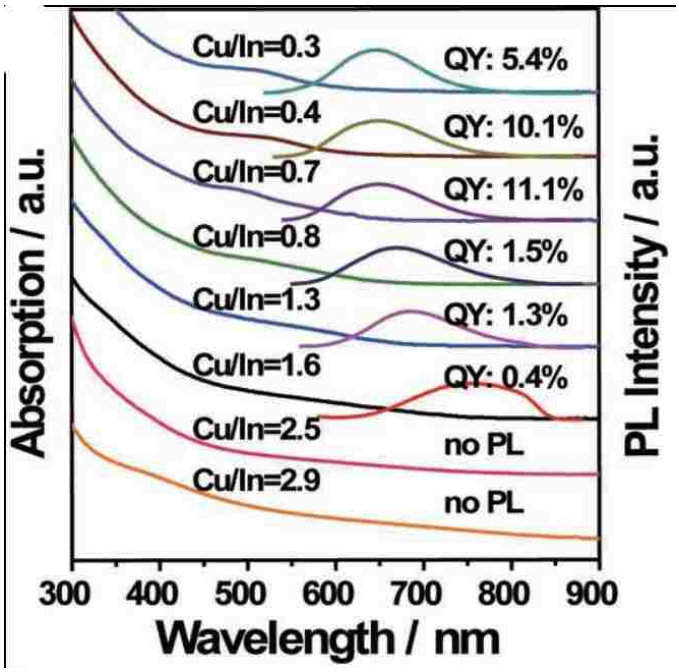

Figure 1.4. Shows how varying the Cu:In ratio can affect the QY. From Chen, B., et al., *Adv. Funct. Mater*., 2012, 22, 2081-2088.[11]

Surface tuning is also accomplished by adding a shell after QD synthesis. CIS and Cd-based quantum dots quite commonly have a ZnS shell since ZnS has a very high band gap, which leads to better charge carrier confinement and surface passivation. However, adding a shell can cause lattice mismatch at the core/shell interface. Large lattice mismatches can lead to an increase in traps states. Depending on the compatibility of the core and shell materials, annealing or ion-exchange may occur, which often leads to a blue-shift in the λ_{max}. On the other hand, if a shell is successfully grown on to the core a small red-shift will occur due to quantum mechanical tunneling of the electron and/or hole wavefunctions from the core into the shell. The lattice mismatch between CIS and ZnS at the core-shell interface is 2.2%.[24] The lattice mismatch in CdSe/ZnS is 12%,[25] while CdSe/CdS has a lattice mismatch of 3.9%.[25] Adding a ZnS shell on CdSe/CdS, forming CdSe/CdS/ZnS QD, allows the large lattice

mismatch between CdSe and ZnS to be distributed amongst multiple interfaces. Even with these additional modifications to CdSe QDs, the lattice mismatch still isn't as low as the CIS/ZnS lattice mismatch, which may lead to different shelling mechanisms in CIS QDs that have not yet been thoroughly investigated. As stated above, cation exchange reactions or inter-diffusional alloying processes may occur for well-matched materials, which may also be used to tune the PL properties.[12] Both of these processes can reduce lattice strain, promote a blue-shift in the λ_{max}, and/or decrease the size of the QD. Alloying occurs when the particle is heated to high temperatures allowing the atoms from the shell lattice to overcome the activation energy to diffuse into the core lattice, and vice versa, leading to a lower energy alloyed single crystal. Cation exchange occurs whereby cations located in the particle are replaced with different cations from the solution, allowing for minimal growth of the particle and minimal lattice mismatch. **Figure 1.5** shows the change in the band gap upon shelling and/or alloying. The Cu-Zn-In-S/ZnS (left) side of the graph blue-shifts as cation exchange and/or annealing is occurring and the Cu-In-S/ZnS (right) side of the graph red-shifts as the shell growths. Finally, there are a number of additional ways to change the PL properties of QDs including changing the ligand,[19] pH,[26, 27] temperature, and other properties of the local environment.[1, 19, 26, 28]

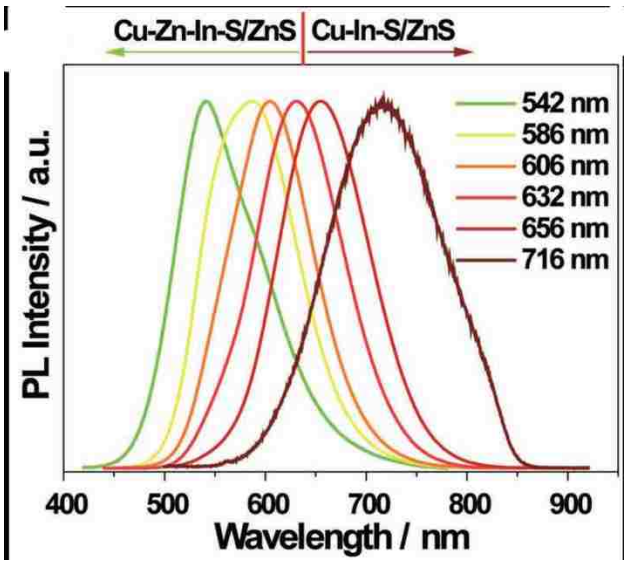

Figure 1.5. Shows how the cation exchange or annealing and shell growth affects the size/band gap of the particles. From Chen, B., et al., *Adv. Funct. Mater*., 2012, 22, 2081-2088.[11]

1.4 Characterizing QDs

There are multiple optical and structural properties of QDs to be measured, which require a wide array of instrumentation. To measure the absorbance spectrum, a UV/Vis absorption spectrometer is used. The main reason to measure the absorbance spectrum is to characterize the band gap of the QD, which can help confirm the QD identity and size. It can be used to measure concentration if the molar absorptivity is known. Measuring the absorbance can also help determine whether scattering is occurring or not. Scattering occurs when the QDs aggregate to sizes approaching the wavelength of the light and appears as a sloping baseline that curves upwards towards lower wavelength. This provides information regarding the colloidal stability of the particles in solution in which they are being measured.

To measure emission and excitation spectra, a photoluminescence spectrometer is used. A lot of information can be obtained from the emission spectrum, such as knowledge about the FWHM, QY, and Stokes shift, when it is combined with the excitation spectrum. The Stokes shift is measured by measuring the distance between the wavelength of the excitation spectrum maximum and the wavelength of the emission spectrum maximum. In **Figure 1.6**, FWHM is measured by determining the intensity at the maximum wavelength (λ_{max}) dividing by two, then determining the distance between the two wavelengths that correspond with that half-maximum value.

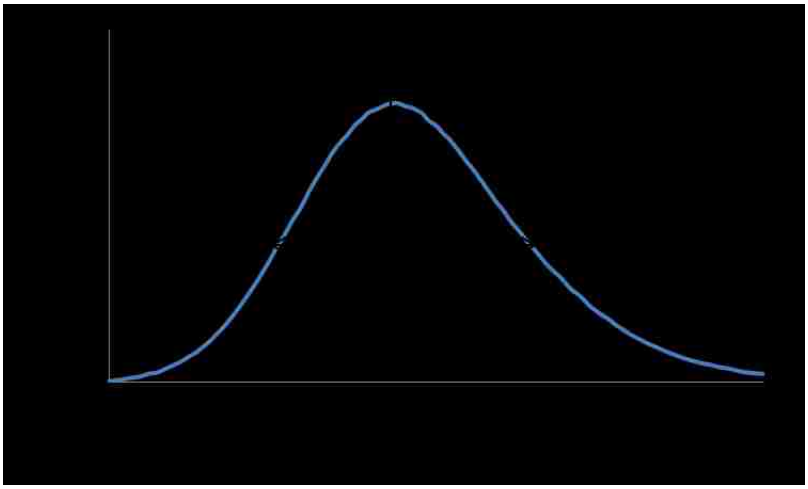

Figure 1.6. A visual illustration of how FWHM is calculated.

QY requires an additional measurement of the emission intensity of a fluorophore that can be excited with the same wavelength and at the same optical density as the QDs being analyzed. Once an appropriate fluorophore is found, integration of both emission spectra is performed. Using **Figure 1.7** as a visual aid for graphical calculation, the integration of the QD is divided by the integration of the fluorophore and then multiplied by the fluorophores known QY value.

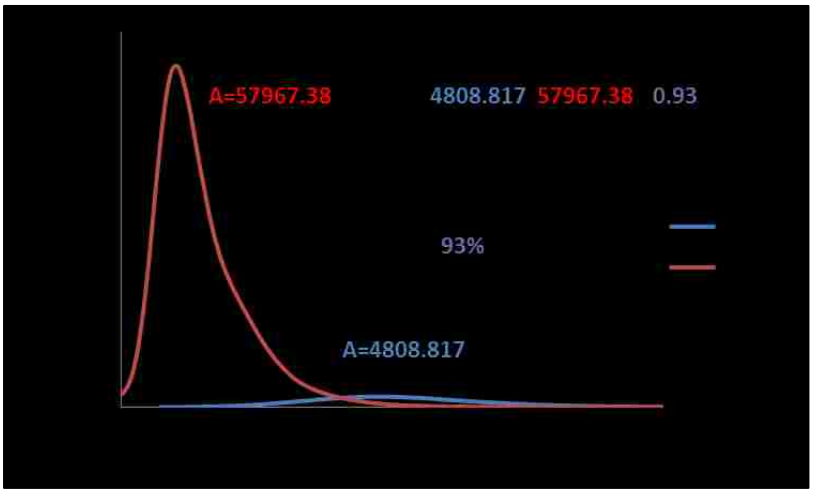

Figure 1.7. A visual example of how QY is calculated

Fluorescence lifetimes, combined with QY are useful to determine the average radiative (k_r) and non-radiative (k_{nr}) rates, which can be used to extract information about the surface defects and trap states. After the lifetime is measured a series of calculations will be done using **Eqn. 2** and **3**.

High radiative rates correlate with high overlap between electron and hole wavefunctions resulting from less trap states being present, and thus leading to higher QYs.[29] A high non-radiative rate means that there are a large number of trap states present or that non-radiative Auger recombination is occurring. Non-radiative Auger recombination is when the energy from an exciton is transferred non-radiatively to either an electron for a negatively charged QD or a hole for a positively charged QD.[5]

Structural analysis is performed by measuring the size, shape, and material composition.[20, 23] High Resolution Transmission Electron Microscopy (HR-TEM) is used to measure the size and shape of the QDs.[11, 20, 23] Inductive Coupled Plasma Mass Spectrometry (ICP-MS) is used to determine the material composition of the QDs.[20, 23] This is especially useful for determining whether ion-exchange,

annealing, or shelling is occurring in the QDs. Standard calibrations curves must be measured on the elements that comprise the QDs being measured.

1.5 Applications of CIS QDs

Some recent applications of CIS QDs that are beginning to be explored are in photodetectors, thermoelectrics and photocatalysis.[13] More specifically, the three main current uses of CIS/ZnS QDs are in light-emitting diodes (LEDs),[12, 13] solar cells,[13] and fluorescent biological imaging.[12, 13] They are great materials for LEDs because their emissions can be finely tuned and they have excellent photostability when a shell is added.[13] Their composition of low toxicity materials makes them ideal for uses in solid-state lighting and display technology where Cd-based QDs are currently being used.[30] They have also received a lot of attention for their promising abilities to produce white-LED (WLED) when combined with certain polymers and films such as YAG:Ce, since they are able to convert part of the blue light that the YAG:Ce is unable to absorb.[31] A study showed that CIS with a QY of 52% was able to maintain 26 lm W^{-1} luminous efficiency with a current of 200 mA over a 40 hour period.[31] Another study has shown that by varying the Zn stearate concentration used for shell growth can optimize the emission for WLEDs even further.[15] With 8 mmol of Zn stearate they were able to obtain a QY of 81%, which led to a luminous efficiency of 60.1 lm W^{-1} at 20 mA and 26.0 lm W^{-1} at 100 mA.[15] It was also found that as the current increased the luminous efficiency decreased. In another study, incorporating a CIS film into a cellulose matrix, which provided good flexibility and was transparent, [32] provided a platform for remote lighting applications.[12]

Many solar cells have used CIS in them because they provide better absorption coefficients and more optimal band gaps than Cd-based QD solar cell models.[13] In a recent study CIS was grown on Ti substrates and then had ZnSe deposited on it to form a solar cell.[33] This solar cell structure under artificial illumination was able to produce an open circuit voltage, V_{oc}, of 325 mV and a short circuit, J_{sx}, of 2 mA cm^{-2}.[33] This was enough to prompt more investigation into using CIS for thin film solar cells. Cu_2S was deposited on a FTO glass covered with TiO_2, then CIS followed by ZnSe, this solar cell is schematically shown in **Figure 1.8**.[34] Under similar conditions, using artificial illumination, this solar cell was able to achieve 2.52% power conversion efficiency.[34]

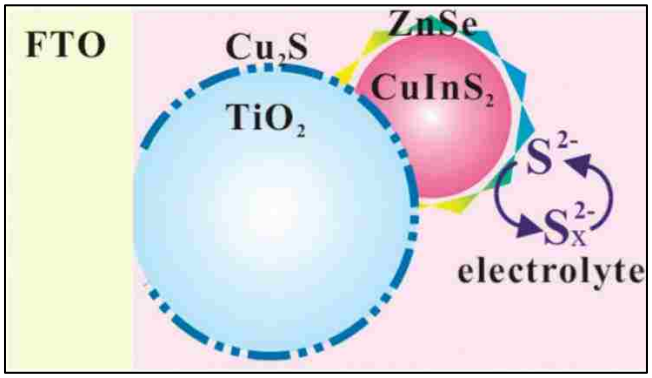

Figure 1.8. Schematic diagram of a Cu_2S/CIS/ZnSe QD-sensitized solar cell. From Chang, J., et al, *Chem. Commun.*, 2012, 48, 4848-4850.[34]

There have been several examples of CIS being used in bioimaging[35, 36] and bioanalysis[16, 37]. The main reasons for these applications are that these QDs are small in size, are capable of near IR emission, are relatively non-toxic and have long fluorescence lifetimes. The capability of being able to tune them to have near IR emission is very important because one can significantly reduce cellular autofluorescence and biological media absorption.[1,12,13] An immunoassay was developed for the detection of mycotoxin aflatoxin B1 using CIS/ZnS.[37] There proved to be a 4-fold higher sensitivity, when compared to a traditional enzyme based immunoassay (ELISA) approach.[37] Another immunoassay study showed the detection of Human Interleukin 6, which is associated with cardiovascular disease.[16] The study showed a detection limit of 0.008 ng mL^{-1}, comparable to conventional ELISA detection limits. CIS is more optimal though because there is only slight interference during detection from nonspecific proteins, such as TNF-α.[16] Many CIS/ZnS bioimaging studies have been performed *in-vitro*, but these *in-vitro* studies show a lot of promise for the eventual transition into *in-vivo* bioimaging. A study from our lab was completed using a time-gated imaging (TGI) method to image human SK-BR-3 breast cancer cells.[35] By using TGI, the cellular autofluorescence was suppressed, improving the signal:noise ratio compared to using conventional dye-based fluorescence imaging. The sub-population of breast cancer cells in the sample was immediately obvious from the images using the QDs, whereas it was more difficult to identify them using fluorescent dyes.[35] CIS/ZnS showed comparable results between CIS/ZnS to CdSe/ZnS,

Figure 1.9. This allows for the replacement of Cd-based QDs with CIS for a non-toxic alternative without losing any of their benefits.

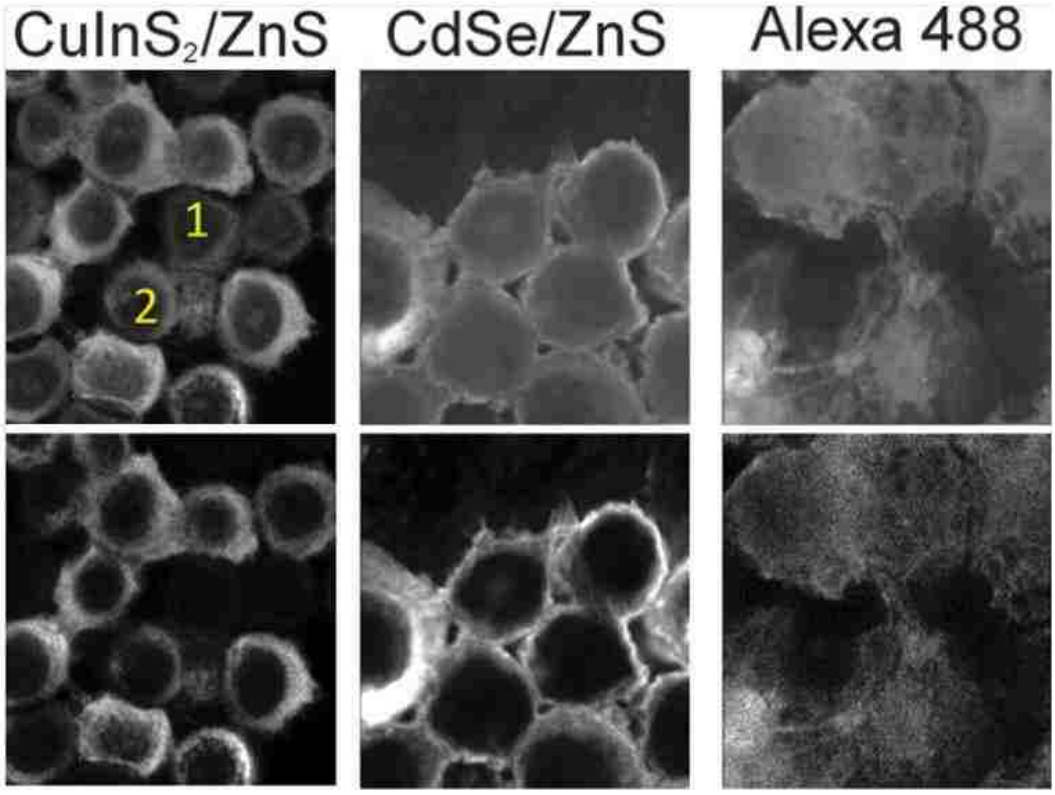

Figure 1.9. The top images are the normal fluorescence intensity images. The bottom row is the TGI images after 10 ns of photons. Comparison of CIS/ZnS, CdSe/ZnS, and the Alexa 488 dye respectively. From Mandal, et al. *Chem. Commun*., 2013, 49, 624-626.[35]

Some CIS/ZnS have been used with additional modifications in order to allow more imaging modalities to be used. One such modification was that CIS/ZnS was doped with Mn to also make them magnetic, in order to be used in magnetic resonance imaging (MRI) for *in-vivo* imaging of tumors.[38] This proved successful for the imaging of tumor cells within 10 minutes of QD injection in mice.[38] A further modification of embedding the QDs into silica beads was performed in order to retain high QYs and allow additional functionality to be imparted.[36] These QDs encapsulated in silica beads ranged in size from 17 to 25 nm and were able to maintain a QY of ~50%. This allowed for the successful detection of HeLa cells using fluorescent imaging and showed that the QDs encapsulated in silica beads could be biofuctionalized by changing the receptors for other cellular bioimaging applications.[36] Clearly, these

examples show that CIS/ZnS are very promising for *in-vitro* and *in-vivo* bioanalysis and bioimaging, and the main aim of this thesis is to further optimize them for such applications.

1.6 Objective of this Thesis

The main focus of this thesis was to better understand the formation of ZnS shells onto CIS QDs for future bioimaging applications, although some of the information gained may also be applicable to solid-state lighting and solar cell applications. The core samples where synthesized using a 1:1 ratio for Cu:In since most literature syntheses have been reported using this condition. The synthesis strategy decided upon was a conglomeration of different protocols. The core synthesis protocol was derived by using a slight variation from Klimov,[39] in which CIS was synthesized at 210°C. A variation from some literature protocols is that DDT was used instead of octadecene (ODE)[37, 40] as the reaction solvent medium.[2, 15, 39] There are many advantages of using DDT as not only the sulfur and ligand component but also as the solvent,[15, 39] including simplicity, less solvent waste, and ensuring that the maximum amount of cation precursors are consumed.[39] The shelling synthesis protocol is the same as developed by the Klimov group.[39] The shelling protocol uses only ODE and not a mixture with oleylamine (OA) as in other protocols,[37, 40] since it is not needed when a copper carboxylate is not being used as the copper precursor.[40] Most shelling syntheses are reported to use between 190 and 210°C,[2, 6, 15, 39, 40] although the role of temperature in the shelling has not yet been studied. Toward this end, we investigate shelling temperatures of 90°C, 130°C, 150°C, 170°C, 190°C, and 210°C in this study. In the study done by Klimov's group, after 20 minutes of shelling at 210°C a λ_{max} of 671 nm and a QY of 67% was obtained.[39] In the study by Song *et al*., after 14 hours at 190°C a QY of 81% and a λ_{max} of 580 nm was obtained.[15] Clearly, shelling temperature plays an important role on the optical properties of CIS QDs, probably via affecting the structural properties of the particles, which is a major focus of this study.

Chapter 2: Experimental Methods

2.1 Chemicals

Copper (I) Iodide (CuI, 98%, Strem Chemicals), Indium (III) Acetate($In(Ac)_3$, 99.99% metals basis, Alfa Aesar), dodecanethiol, (DDT, 98%, Aldrich), 1-octadecane (ODE, 90%, Alfa Aesar), zinc stearate ($C_{36}H_{70}O_4Zn$, Acros), sulfur powder (S, 99.5%,sublimed, -100 mesh, Alfa Aesar), trioctylphosphine, (TOP, 95%, Alfa Aesar). Hexanes (GR ACS) and methanol (HPLC Gradient Grade) were purchased from VWR International.

2.2 Synthesis of CIS

1.0 mmol of $In(Ac)_3$, 1.0 mmol of CuI, and 20.9 mmol of dodecanethiol (DDT) were added to a 3-neck 25 mL round bottom flask (rbf).The DDT acts as the sulfur precursor, the ligand for the QDs as well as the solvent medium. The temperature was controlled using a Digi-sense digital thermometer (Cole & Parmer) with an Omega thermocouple probe (Type K, 12 inches). The solution is then degassed under vacuum for 5 minutes and then purged with argon for 5 minutes; this process is repeated 3 times. The reaction remains under constant flow of argon and the solution is slowly heated to 100°C and held at this temperature for 10 minutes. The solution then turns a clear yellow color, after which it is slowly heated to 210°C. Once it turns deep red in color, a timer is started. The core synthesis was performed for 35 minutes.

2.3 Synthesis of CIS/ZnS

1 mL of the concentrated, newly-synthesized core and 4 mL of ODE were added to a 3-neck 50 mL rbf. The solution was degassed under vacuum for 5 minutes and purged with argon for 5 minutes; repeated three times. The shelling precursor was made up by adding 0.4 mmol zinc stearate and 4 mL of ODE to a 3-neck 25 mL rbf. This flask was degassed under vacuum for 10 minutes and purged with argon for 5 minutes. A separate solution was made in a vial by adding 0.4 mmol of sulfur powder and 0.4 mL of TOP and sonicated for 20 minutes, which was then added to the reaction. Once the sulfur solution was added to the 25 mL rbf, the flask was degassed under vacuum for 5 minutes and then kept under constant argon until it was ready to be transferred to the 50 mL rbf containing the core. Once the 50 mL

rbf was finished degassing and purging, the temperature was slowly raised up to the selected shelling temperature (210°C, 190°C, 170°C, 150°C, 130°C, 90°C). Once the QD solution had reached the selected shelling temperature, the addition of the shelling precursor solution in the 25 mL rbf was added drop-wise over 20 minutes (approximately 0.2 mL/min). When the shelling precursor addition began, a timer was started. The samples were taken from the reaction at various time intervals of 20, 30, 40, 50, 60, 80, 110 and 140 minutes. In a separate experiment, a second injection of the shelling precursor materials is added 30 minutes after the first.

2.4 Optical Spectroscopy

The samples' absorbance spectra were measured by diluting in hexane until an optical density of 0.1 at 485 nm for each was obtained; this was done to ensure that all the measurements would be under the same conditions so a pattern could more easily be recognized. If scattering was present, the samples were centrifuged twice at 4000 rpm for 30 minutes to remove any aggregates. A Hitachi U-3900H UV/Vis spectrophotometer with a 1 cm quartz cuvette was used to measure the absorbance spectra. The spectra were obtained between the wavelengths of 400 to 800 nm. Although the QDs do not absorb after 700 nm, the spectra was measured to 800 nm to ensure that the baseline was flat, indicative that no scattering was occurring from aggregated particles.

Once an optical density of 0.1 at 485 nm was obtained for the samples, the emission spectra were measured on a Perkin Elmer LS55 Luminescence Spectrometer, also using a 1 cm quartz cuvette. The excitation wavelength for the emission spectra was 485 nm to match the laser available for the fluorescence lifetime measurements that will be measured afterwards. The photoluminescence excitation (PLE) measurements were performed on the same instrument, using the obtained emission λ_{max} of the specific sample as the emission wavelength at which the PLE spectrum is measured.

The fluorescence lifetime measurements were obtained on the same samples using a Picoquant Micro Time 200 Fluorescence Lifetime Microscope with a Pico Harp 300 TCSPC Module and Picosecond Event Timer. A 485 nm laser (LDH485 controlled using a Sepia II mulitchannel picosecond diode laser controller) was used for excitation and a long-pass emission filter of 510 nm was used to filter out the scatter laser light in the detection path. The pulse rate was set to 800 kHz, to ensure that the excited QDs

had enough time between pulses to fully relax back down to ground state before re-excitation in order to limit incorrectly measured lifetimes due to multiphoton absorption.

2.5 Transmission Electron Microscopy (TEM)

In order to prepare a sample for TEM measurement, the QDs were washed, centrifuged and re-suspended to remove all soluble impurities in the QDs. This was done by dissolving approximately 100 μL of the concentrated, unpurified sample in equal parts of hexanes and methanol. The sample was shaken to ensure it was dispersed and then put in the centrifuge at 4000 rpm for 30 minutes. Once centrifugation was complete the QD sample had formed a pellet on the bottom of the vial and the excess solvent was carefully removed, it was then re-suspended in solvent. The process was then repeated three times for each sample prepared. The TEM samples were prepared by adding the solution drop-wise to a TEM grid (400M Ni grids with carbon film) using 10 μL aliquots to a total of 100 μL. The samples were then left to air dry for at least 30 minutes, and then dried in the storage box for 24-72 hours to ensure complete dryness. The samples were plasma cleaned for 30 seconds and images obtained using the TEM, FEI Titan 80-300 that is hosted at the Institute for Nanoscience and Engineering located on the University of Arkansas, Fayetteville campus. The images were obtained using a 300 kV acceleration voltage and magnification between 600,000- 1,200,000x.

2.6 Inductively Coupled Plasma- Mass Spectrometry (ICP-MS)

Before ICP-MS was performed on the QDs, calibration curves were taken using Cu, In, and Zn standards. Sulfur could not be measured due to it being present in both the QD and the coordinating ligand. Calibration curves were set up using concentrations of 1, 10, 50, and 100 ppb with the standards being diluted using 2% HNO_3. Once successful calibration curves were obtained, QD solutions for which TEM images had been taken, were prepared after the QDs were purified. The same purification process as described above was applied to sample purification for ICP-MS. The purified samples were dissolved in minimal amounts, as in a few drops, of concentrated HNO_3 and diluted with 2% HNO_3 to ensure that the concentrations fell within the 1-100 ppb range that provides the optimal accuracy on the instrument. ICP-MS was performed on a Thermo iCAP QC (Bremen, Germany) using 2% HNO_3 as the baseline

standard and washing solution, the solutions were analyzed in kinetic energy discrimination (KED) mode, which uses He as a collision cell gas to remove polyatomic interferences.

Chapter 3: Results & Discussion

3.1 Results

3.1.1 Optical Properties

3.1.1.1 Absorbance and Excitation Spectroscopy

Figure 3.1 shows an example of the absorbance spectrum of CIS/ZnS. The curve shows no peak, but rather a gradual increase of absorbance after 700 nm with a slight plateau in the 450-550 nm range. The flat baseline between 700–800 nm indicates that no scattering is occurring and that the QDs do not form large aggregates in solution.

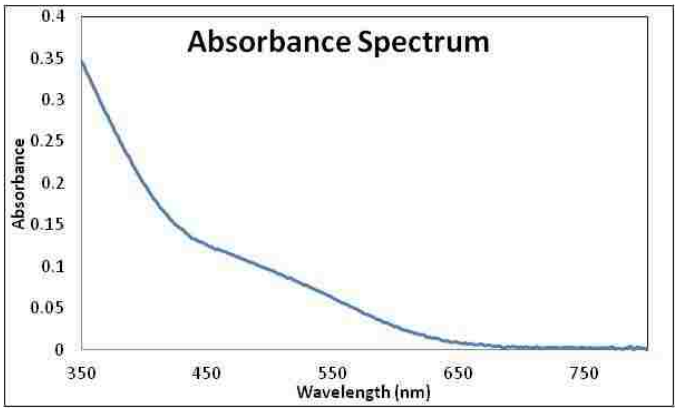

Figure 3.10. Example Absorbance spectrum of CIS/ZnS.

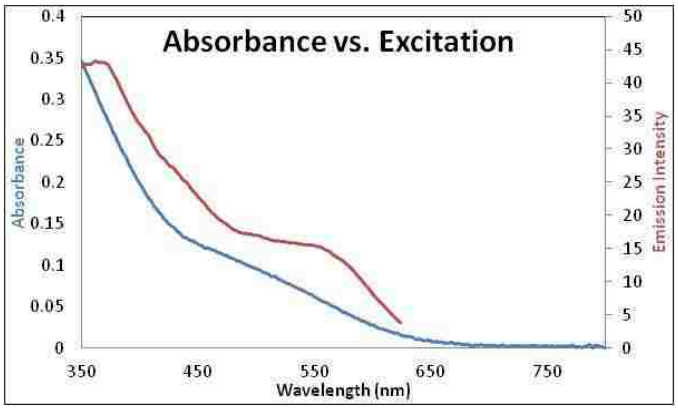

Figure 3.2 Comparison of the absorbance spectrum with the excitation spectrum. Both spectra are the first 190°C shelling at 50 minutes.

The comparison of the absorbance and the excitation spectra is shown in **Figure 3.2** with both curves having the same general shape. The excitation curve has a better defined plateau around 550 nm. The excitation spectrum resolves the band edge electronic states better than the absorption spectra. This is possibly due to direct absorption of the QDs into non-emitting trap states. It has been previously discussed that CIS QDs have a very broad emission spectra because they contain more than one kind of emission center.[2]

3.1.1.2. Photoluminescence Spectroscopy

There are many properties that can be determined from the photoluminescence spectra, including the maximum wavelength (λ_{max}), the quantum yield (QY), and the full width at half maximum (FWHM). This can be seen in **Figure 3.3** in which, a blue shift of the λ_{max} can be observed as the shelling time (and number of injections of precursor) increases, as well as an increase in the emission intensity and FWHM.

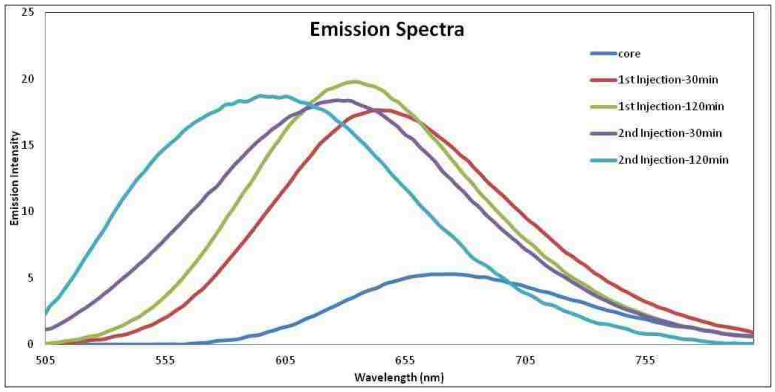

Figure 3.3. A comparison of the emission spectra for the shellings at 190°C to show general blue-shifting of λ_{max}, increasing PL intensity, and increasing FWHM.

A comparison of the difference between the absorbance/excitation spectrum λ_{max} and the emission spectrum λ_{max}, can also be used to calculate the Stokes shift. In **Figure 3.4** the Stokes shift for CIS is calculated to be 90 nm.

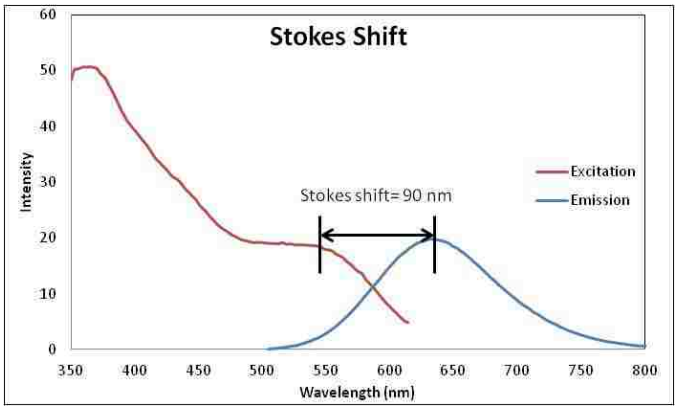

Figure 3.4. The Stokes shift for CIS/ZnS during the first shelling at 190°C after 140 minutes.

Figure 3.5 A and **Figure 3.5 B** shows the reproducibility in the PL properties for 3 separate syntheses of CIS and CIS/ZnS was achieved. This is shown by comparing the PL intensity, λ_{max}, and FWHM. The PL intensities, λ_{max}, and FWHM values are all very close to one another.

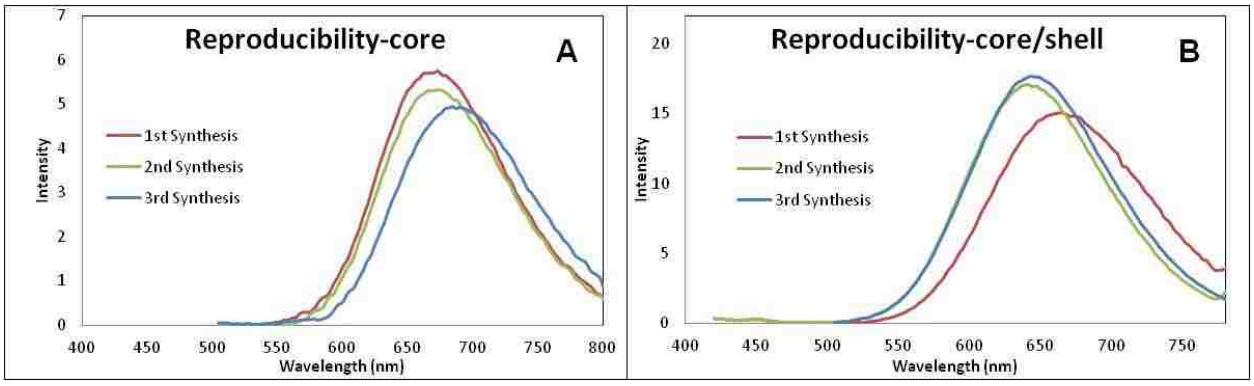

Figure 3.11. The PL spectra of (**A**) 3 cores and (**B**) 3 core/shells synthesized. The core samples were all performed for 35 minutes at 210°C. The core/shell synthesis samples were synthesized at 190°C with all samples taken at 30 minutes after shell precursor injection.

3.1.1.2.1 Blue-shift

The blue-shifting of the λ_{max} occurs for all samples, independent of shelling temperature, although the degree of the blue-shift does depend on the shelling temperature. **Figure 3.6** shows that, as the temperature decreases, so does the degree of the λ_{max} blue shift. The largest change can be seen at 210°C. The largest blue-shift occurs during the 20 minute injection time, but then continues to decrease slowly over two additional hours. If a second injection of precursors is added after 30 minutes of finishing

the first injection, a strong blue shift occurs again, which also continues to decrease for another 2 hours. At lower temperatures, the same trend is observed, although the extent of the blue-shift reduces, especially at longer time and after the second injection. At 90°C there is still a moderate blue-shift over the 20 minute injection period, but no further shift is observed over the next hour. Adding a second injection of shelling precursors does not lead to an additional blue-shift at all at this temperature.

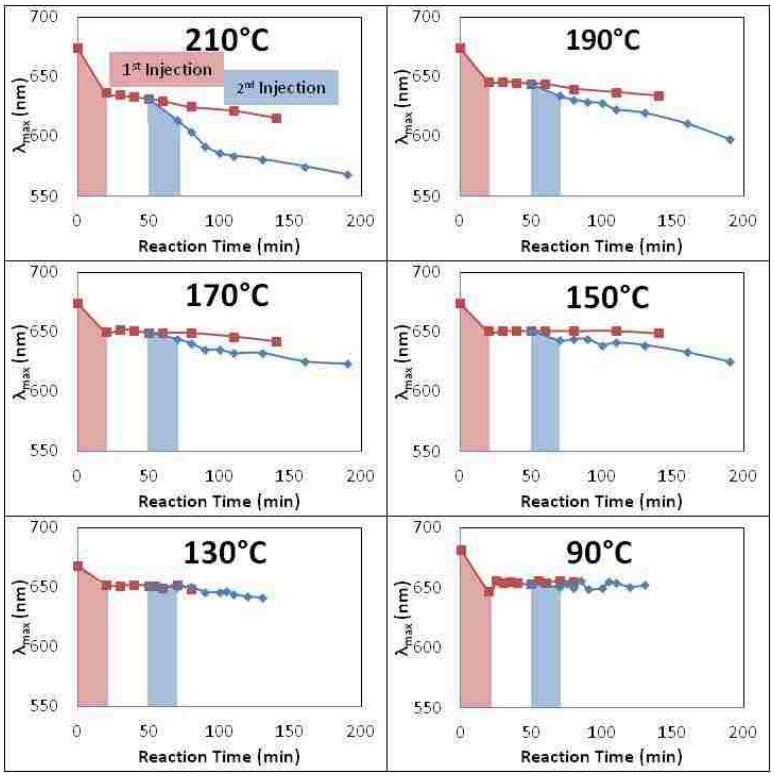

Figure 3.6. The λ_{max} blue-shift as a function of shelling time and temperatures with only one injection (red) and a second injection 30 minutes after the first (blue) of the Zn and S shelling precursors. The shaded red and blue areas correspond to the time it took to add the Zn and S shelling precursors during the 1st and 2nd injections, respectively.

3.1.1.2.2 Photoluminescence and Quantum Yield

The resulting photoluminescence quantum yield (QY) is also dependent upon the shelling temperature and reaction time. It can be seen from **Figure 3.7** that there is always an increase in the QY with the first injection, with the extent of the increase depending on the shelling temperature. The higher the shelling temperature was, the greater the change in the QY.

While there is always an increase in QY with the first injection, there is not always an increase in QY with the second injection. The second injection can cause either an increase or a decrease in the QY

depending on the temperature. At 210°C, there is an obvious decrease in QY with the second injection. For temperatures between 190°C and 150°C, there is always an initial decrease in the QY with the second injection but, over the next two hours, there is a steady increase in the QY so that it eventually surpasses the QY from only one injection. At 190°C, the QY eventually starts to decrease at prolonged times after the second injection. At the 130°C and 90°C, the second injection causes an immediate increase in the QY, although it is only minimal, and continues to rise only very slowly with time. Clearly a minimum temperature of 150°C is needed for the injection of Zn and S to have any significant effect on the PL of the CIS QDs, with two injections at 190°C and a total shelling time of ~150 minutes provides the highest QY.

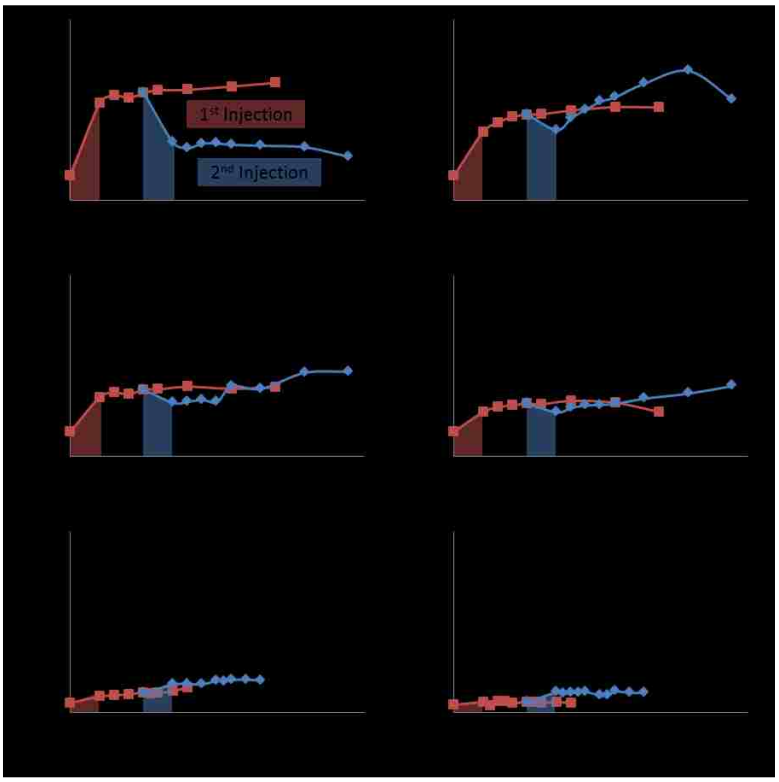

Figure 3.7. The change in quantum yield (QY) as a function of shelling time and temperature with only one injection (red) and a second injection 30 minutes after the first (blue) of the Zn and S shelling precursors. The shaded red and blue areas correspond to the time it took to add the Zn and S shelling precursors during the 1st and 2nd injection, respectively.

3.1.1.2.3 Full Width at Half Maximum

Figure 3.8 shows the full width at half maximum (FWHM) values, which are also dependent upon shelling temperature. While the first injection does not significantly affect the FWHM, remaining between 115 and 120 nm, the second injection results in varied effects, depending on temperature. At 210°C, the FWHM starts to decrease over time, following an initial increase during the injection time, while at lower temperatures the FWHM values increase over time. The degree of this increase is temperature dependent. The lower the temperature, the smaller the degree of increase was until there was no change at 130°C or below.

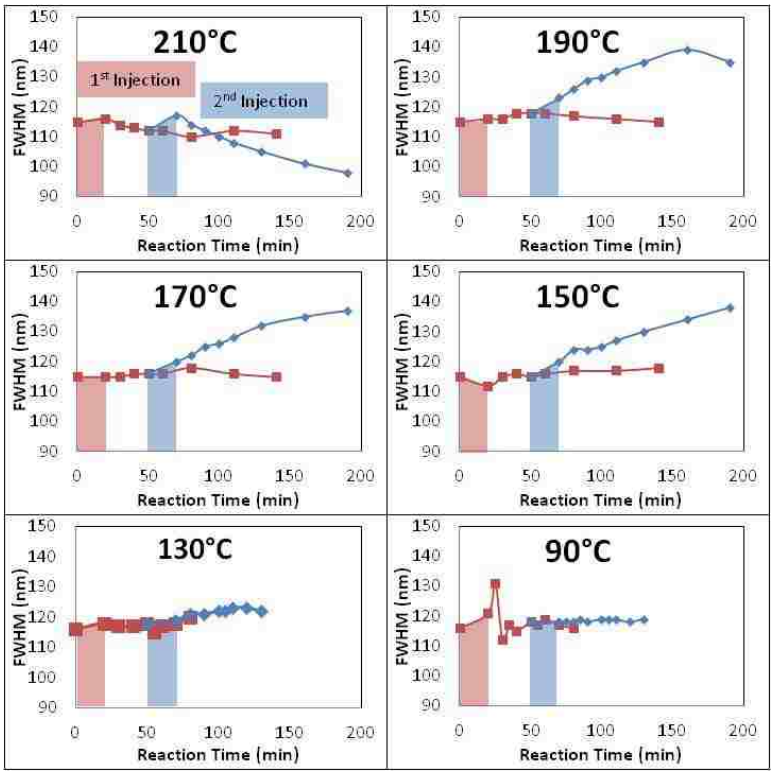

Figure 3.8. The change in full width at half max (FWHM) as a function of shelling time and temperature with only one injection (red) and a second injection 30 minutes after the first (blue) of the Zn and S shelling precursors. The shaded red and blue areas correspond to the time it took to add the Zn and S shelling precursors during the 1st and 2nd injection, respectively.

3.1.1.2.4 Fluorescence Lifetime, Radiative Rate, and Non-radiative Rate

The average fluorescence lifetime for each temperature is shown in **Figure 3.9** and demonstrate that temperature had the general effect of decreasing the lifetime of CIS from ~250 ns at 210°C to ~190ns at 90°C, although it was not strongly affected by the shelling (either the number of injections of precursors or the shelling time), with a couple of exceptions. Interestingly, at lower temperatures (between 150°C

and 90°C), the first injection caused a slight decrease in the fluorescence lifetime during the injection time by about 20%, but the second injection did not. On the other hand, at 210°C the first injection did not affect the lifetime but the second injection caused a decrease in the average fluorescence lifetime from ~250 ns to ~190 ns (about 30%).

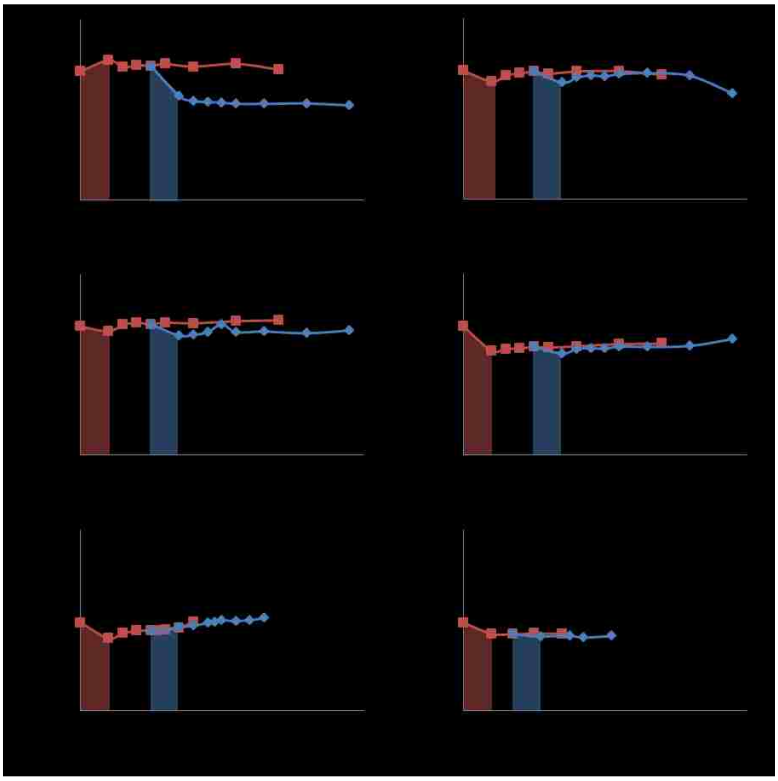

Figure 3.9. The change in fluorescence lifetime as a function of shelling time and temperature with only one injection (red) and a second injection 30 minutes after the first (blue) of the Zn and S shelling precursors. The shaded red and blue areas correspond to the time it took to add the Zn and S shelling precursors during the 1st and 2nd injection, respectively.

The fluorescence lifetime (τ_{fl}) and QYs allowed us to calculate the average radiative and non-radiative rates using the equations below:

$$k_r = \left(\frac{QY}{\tau_{fl}}\right) \qquad \textbf{Eqn. 1}$$

$$k_{nr} = \left(\frac{1}{\tau_{fl}}\right) - (k_r) \qquad \textbf{Eqn. 2}$$

Figure 3.10 shows that as the shelling temperature decreased so did the radiative rate, while the non-radiative rate showed an increase. The radiative rate during the first shelling injection tends to increase, with higher temperatures having a greater degree of increase, and then continues to increase

slowly with time. The second shelling injection caused the radiative rate to either decrease or increase depending on the temperature. At 210°C it decreases significantly, but at 190°C-90°C they all increase, after an initial small decrease, with the degree of increase depending on the actual temperature. Higher temperatures lead to a greater increase during the second injection than the lower temperatures, as long as the temperature does not go above 190°C.

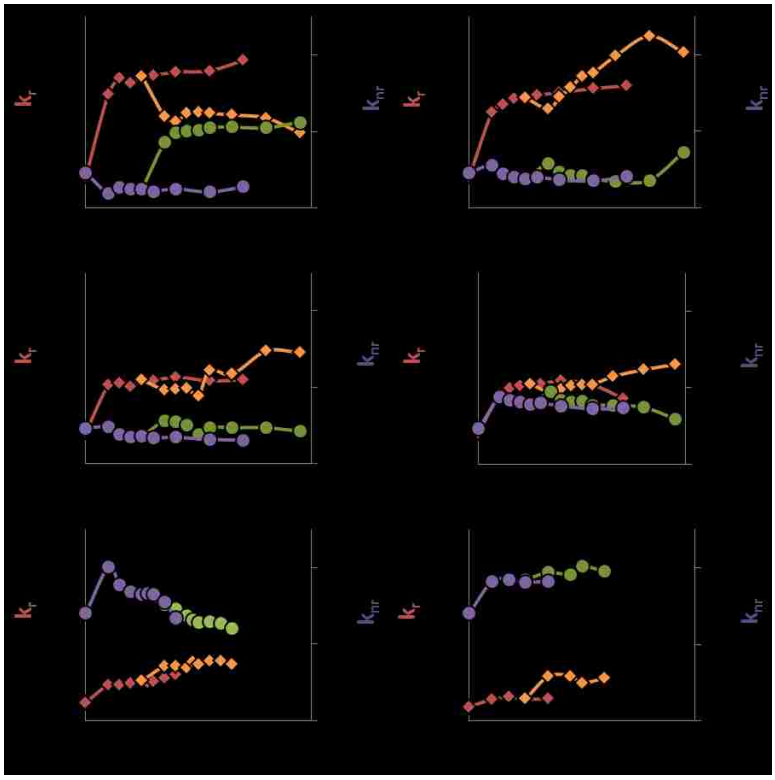

Figure 3.10. The graphs show the radiative (k_r) and non-radiative rates (k_{nr}) for the lifetimes over time at various temperatures. The change in color for the radiative (red to orange) and non-radiative (purple to green) data indicates the second injection of shelling precursors.

The non-radiative rate for temperatures between 210-170°C have little change over time after the first sample is taken for the first injection, which decreases for 210°C and increases for 190-170°C. At 150°C there is also little change in the non-radiative rate over time but the first sample increases significantly compared to the increase that occurred for 190-170°C. The lower temperatures, 130-90°C, have significantly higher non-radiative rates than the other temperatures, with the sample at 130°C first increasing then decreasing. The first injection at 90°C shows an increase of the non-radiative rate, then remains constant over time. The second shelling injection leads to increase in the non-radiative rate at

210°C, but remains relatively constant when shelling is performed between 190 and 170°C. However, at 150-130°C, the second injection leads to a continuation in the decrease in the non-radiative rate that resulted from the first shelling, with 130°C showing a stronger decrease. At 90°C, the second injection did not affect the non-radiative rate.

3.1.2 Structural Properties

3.1.2.1 TEM Size Analysis

The structural properties were investigated by measuring the size of the particles via TEM. **Figure 3.11** shows the low magnification TEM images at the highest three shelling temperatures following one or two shelling injections. They all indicate that the particles are spherical in shape. The high magnification images of a single QD inset in the low magnification images also show the lattice fringes indicative of high crystallinity materials. **Figure 3.12** shows the histograms for the particles shelled at these temperatures following one or two shelling injections. The average sizes were between 2.7 and 3.2 nm in diameter.

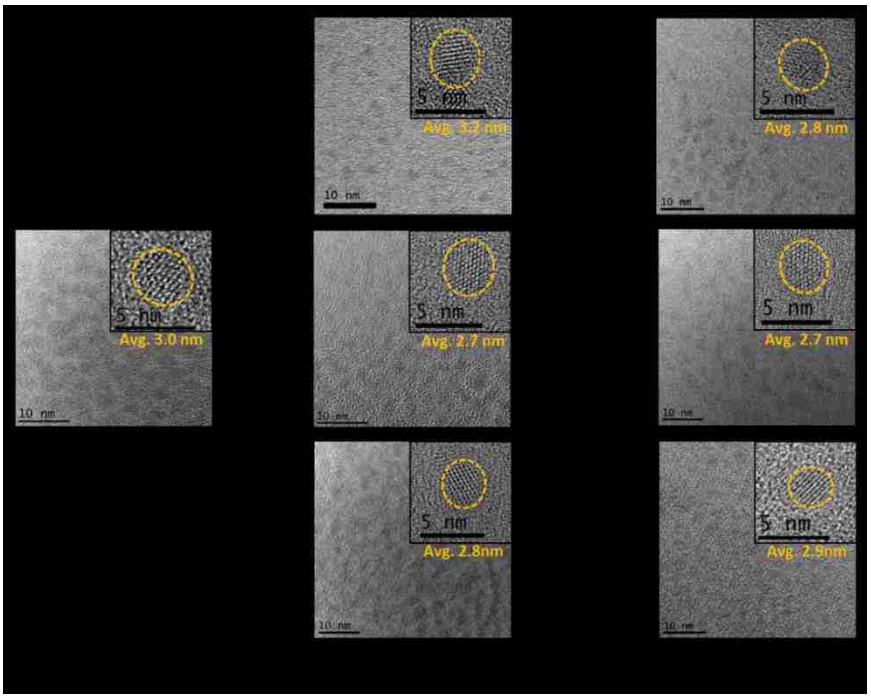

Figure 3.11. Low magnification TEM images displaying the overall spherical shape of the particles together with high magnification TEM images of single particles (inset).

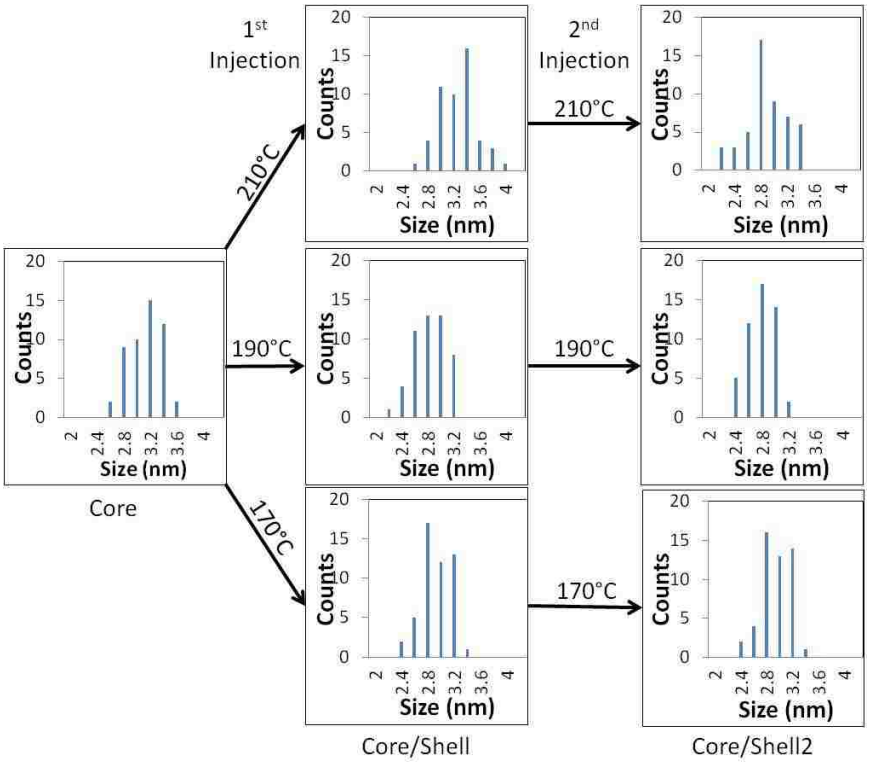

Figure 3.12. Size distribution histograms of CIS/ZnS QDs for particles shelled at different temperatures and number of injections of shelling precursors.

3.1.2.2 Elemental Composition

Since the QDs did not increase in size upon adding ZnS, ICP-MS was used to determine the elemental composition upon adding Zn and S precursors to CIS QDs to evaluate the degree on ion-exchange or annealing occurring between the various materials. The concentrations of Cu, In, and Zn were determined. It was not possible to determine sulfur composition due to interference from the sulfur-containing coordinating ligands (dodecanethiol) used during synthesis. **Figure 3.13** shows the percent composition of these elements in the QDs at various time points during reaction at the different shelling temperatures.

The 210°C shelling is significantly different than the other two temperatures in that the Zn composition remains reasonably high after prolonged times, and continues to remain at this level after a second injection of the Zn and S shelling precursors. The percent composition data after the first injection shows that Zn increased significantly for all the temperatures within 60 to 90 minutes after the first

injection. The composition following the second injection shows a slight increase in Zn, a decrease in In but, surprisingly, an increase in the Cu composition at 210°C. At 190°C and 170°C the percent compositions of Cu and In present in the QD after the first injection first decreased but then increased at longer times. Concurrently the composition of Zn first increased, but then decreased at longer times. Even more surprisingly, the second injection of Zn and S precursors led to a continuing decrease in the amount of Zn in the QD. The amount of In also decreased but the amount of Cu increased. Clearly, the amount of Zn that can be incorporated into the QD at temperatures lower than 210°C is already saturated after the first injection and, moreover, is reversible.

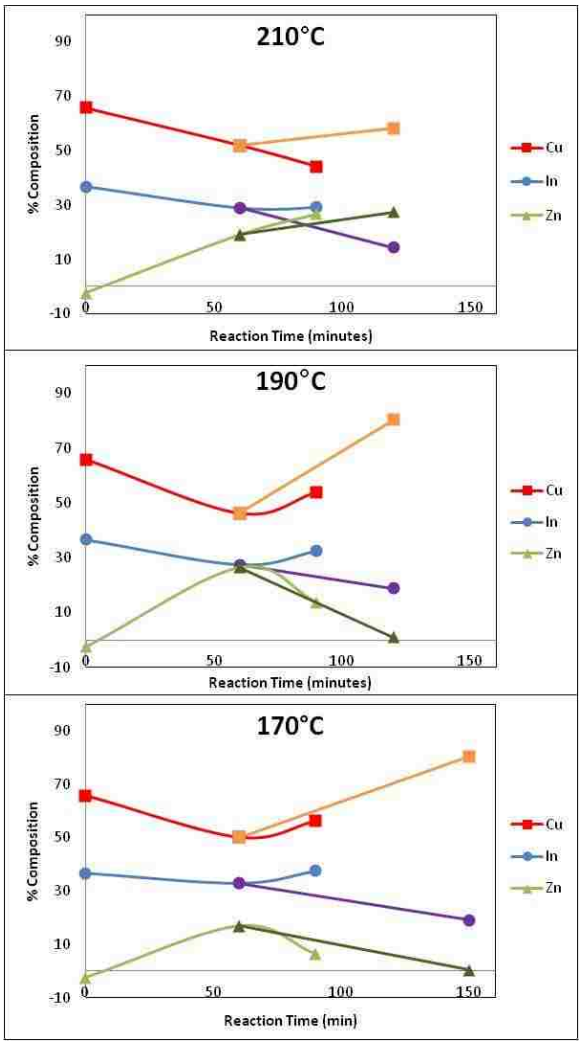

Figure 3.13. The ICP-MS results showing % relative composition of Cu, In, and Zn for the particles at various times after injection of Zn and S at various temperatures. The color change indicates the second injection. (red to orange: Cu, blue to purple: In, green to dark green: Zn)

3.1.3 Bi-temperature Shelling

Since the results above showed that the first injection at 210°C led to the largest increase in QY, but that a larger increase in QY was found during the second injection at 190°C than 210°C, we decided to test if we could obtain better QYs if the second injection was performed at a different temperature than the first, which we term "bi-temperature shelling". The first injection was performed at 210°C and the second injection was performed at either 90°C or 190°C. The various properties of λ_{max}, QY, FWHM, lifetime, radiative and non-radiative rates, and TEM images were measured and calculated.

3.1.3.1 Photoluminescence Spectroscopy

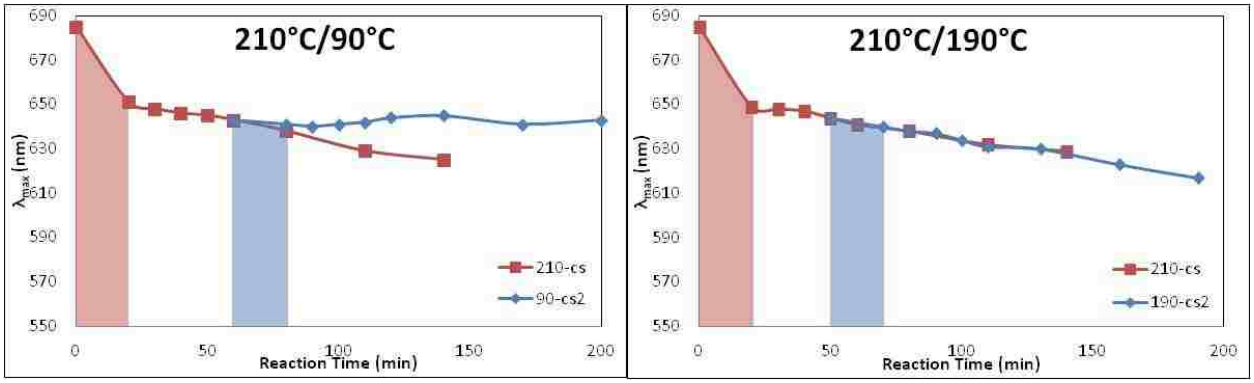

Figure 3.14. The λ_{max} blue-shift as a function of time and number of injections for the two bi-temperature shelling studies. The shaded red and blue areas correspond to the injection time of the Zn and S shelling precursors.

Figure 3.14 shows the λ_{max} shift. After the first injection it still blue-shifts, as expected, but as the temperature is reduced to 90°C and a second injection given, there is no further shift. When the second injection is given at 190°C, the blue-shift continues with the same rate as that at 210°C.

The first injection at 210°C led to an increase in QY, as expected, as shown in **Figure 3.15.** A second injection at 90°C led to a decrease in QY over time at the same rate as if the temperature was maintained at 210°C without an additional injection. The second injection was done at 190°C, there was initially a slight decrease in the QY followed by an increase over two additional hours, at which it started to decrease again. This was identical to the behavior seen above when the temperature was maintained

at 190°C for both injections. The highest QY was obtained from the 210°C/190°C bi-temperature shelling over a 150 minute reaction time, with a QY of 11.1%.

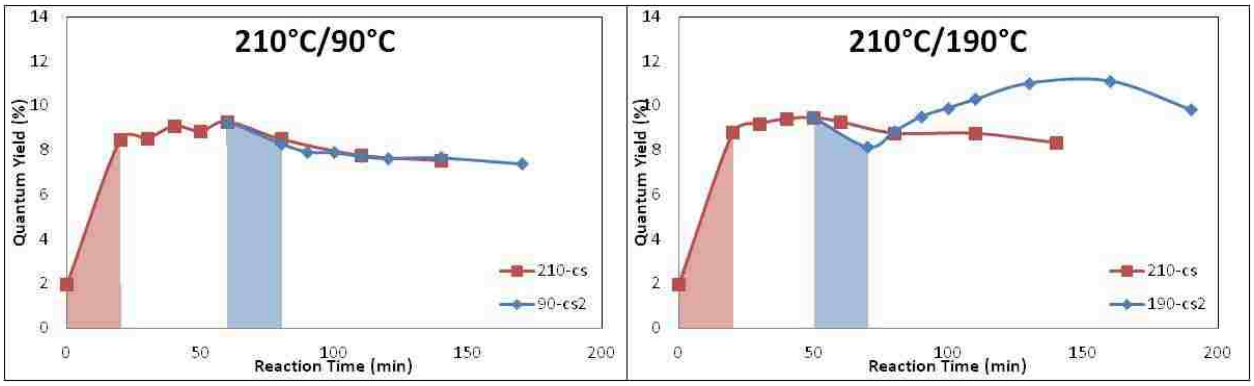

Figure 3.15. The change in quantum yield (QY) as a function of time and number of injections for the two bi-temperature shelling studies. The shaded red and blue areas correspond to the injection time of the Zn and S shelling precursors.

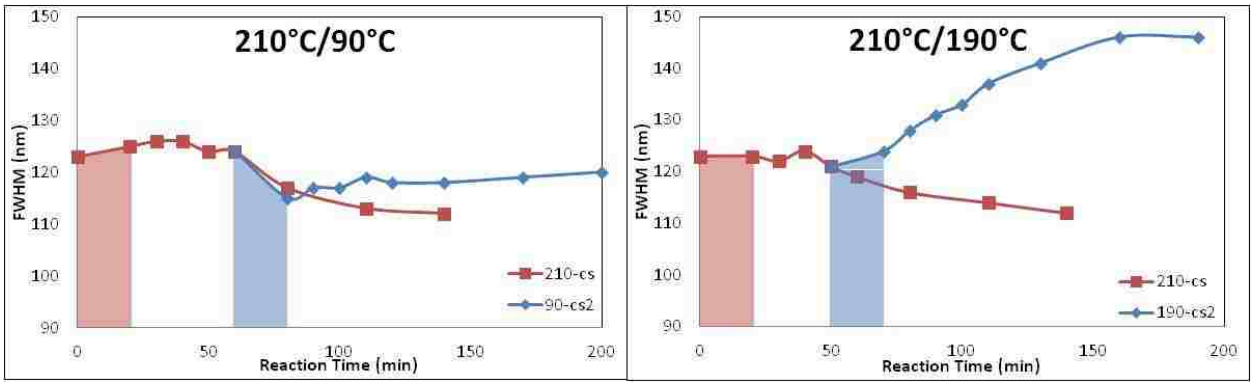

Figure 3.16. The change in FWHM as a function of time and number of injections for the two bi-temperature shelling studies. The shaded red and blue areas correspond to the injection time of the Zn and S shelling precursors.

The FWHM data for the two bi-temperature studies are shown in **Figure 3.16**. At 210°C, there is decrease in the FWHM at longer shelling times but lowering the temperature to 90°C and providing a second injection halted this decrease. On the other hand, a second injection at 190°C led to a continual increase in the FWHM, which began to plateau after ~150 minutes.

3.1.3.2 Fluorescence Lifetime, Radiative Rate, and Non-radiative Rate

Figure 3.17 shows the fluorescence lifetimes for the bi-temperature shelling studies which, as before, showed little effect on either temperature or injection number. The 210°C/90°C study showed

consistent lifetime values after the first injection, whereas the 210°C/190°C study led to a slow decrease in the fluorescence lifetime with time but did not depend on whether a second injection was giver or not.

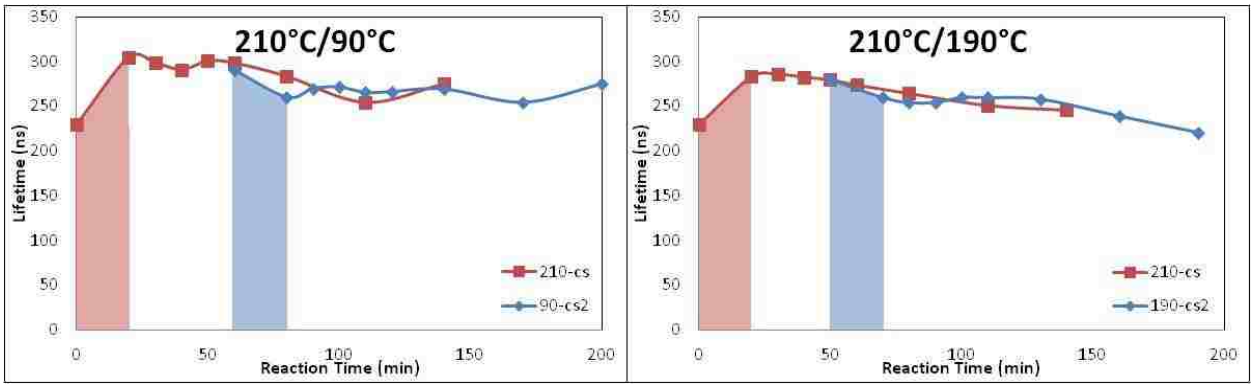

Figure 3.17. Fluorescence lifetime as a function of time and number of injections for the two bi-temperature shelling studies. The shaded red and blue areas correspond to the injection time of the Zn and S shelling precursors.

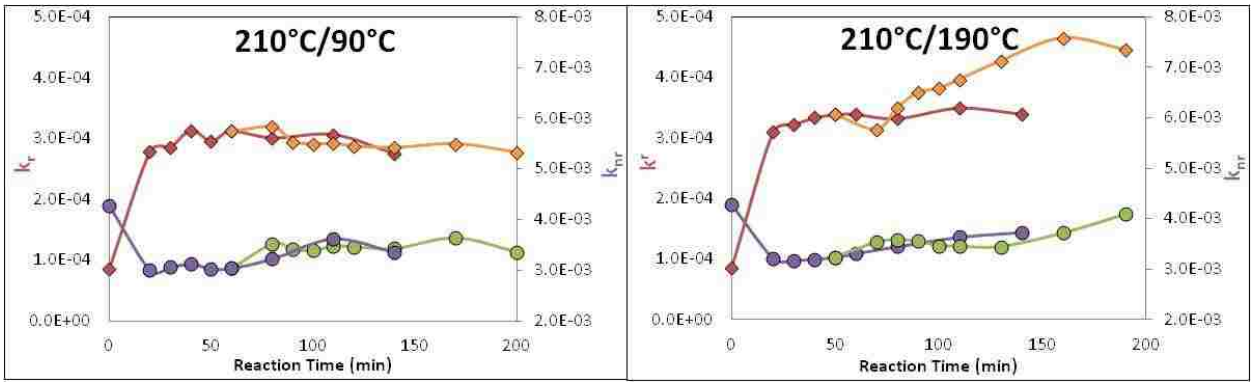

Figure 3.18. The graphs show the radiative and non-radiative rates for the lifetimes over time for the two bi-temperature shelling studies. The change in color for the radiative and non-radiative data indicates the addition of another injection of precursors. The red and purple are done at 210°C and the orange and green are done at either 90°C or 190°C.

Using the lifetime values and the QY for these samples the radiative and non-radiative lifetimes were calculated as described above. **Figure 3.18** shows the 210°C first injection led to the same increase in the radiative rate and decrease in the non-radiative rate during the injection period as the single temperature studies. For a second injection at 90°C the lifetime remained constant, which is different from single temperature shelling in that the radiative rate was significantly higher and nonradiative rate was significantly lower. When the second injection was given at 190°C, it led to the same shape as observed in the single temperature study. The radiative rate increased more rapidly over time after the second

injection than it did for the single injection at 210°C. The non-radiative rate increased slightly, although at the same rate as if there was only one injection at 210°C.

3.1.3.3 TEM Size Analysis

Figure 3.19 shows the low magnification and high magnification TEM images synthesized in the 210°C/190°C bi-temperature study. The low magnification images show that the general shape of the QDs are spherical. In the high magnification images the lattice structure can be seen, again showing the excellent crystallinity of the QDs.

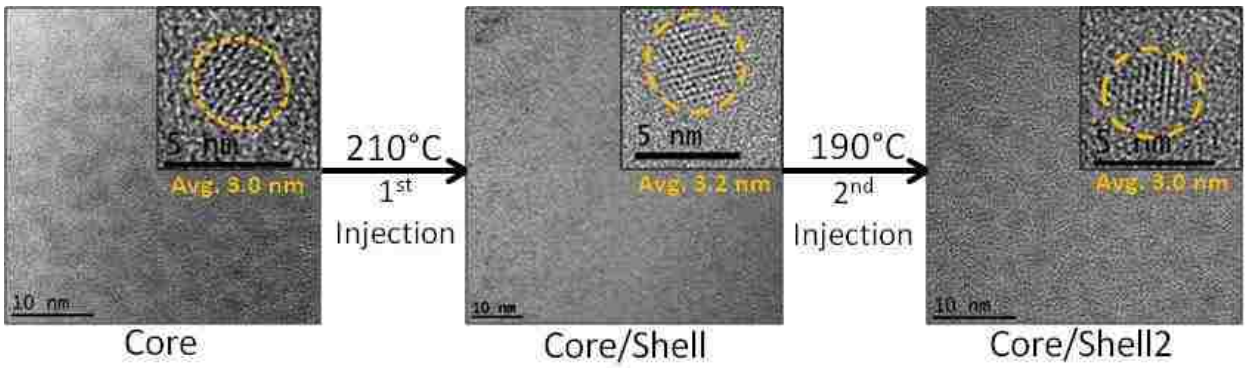

Figure 3.19 Low magnification TEM images displaying the overall spherical shape of the particles together with high magnification TEM images of single particles (inset) for QDs synthesized via the 210°C/190°C bi-temperature shelling procedure.

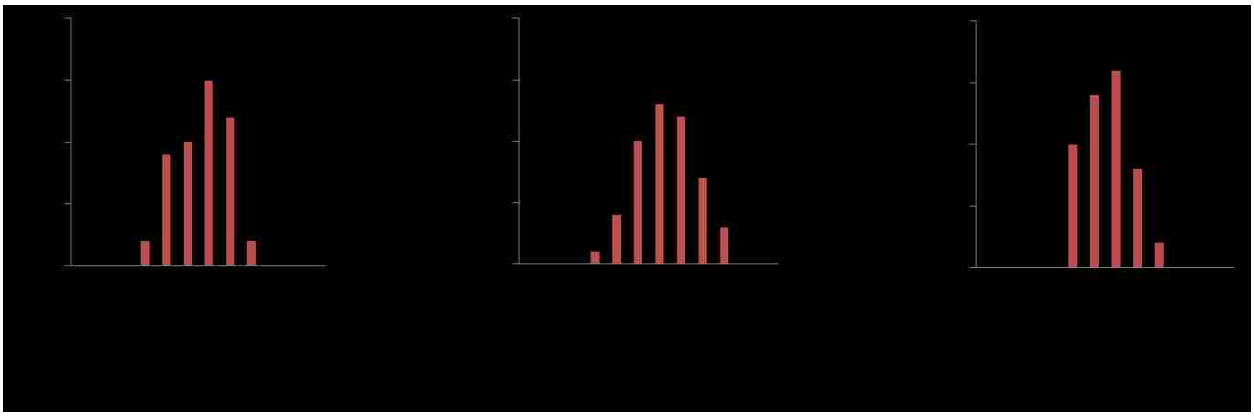

Figure 3.20. Size distributions histograms of CIS/ZnS QDs for the particles synthesized via the 210°C/190°C bi-temperature shelling procedure.

The histograms for the 210°C/190°C bi-temperature study are shown in **Figure 3.20**. The average size between the core and the second shelling at 190°C averaged in size between 3.0 and 3.2 nm in diameter with no change after either one or two injections.

3.2 Discussion

3.2.1 First Injection

At the highest shelling temperature, 210°C, there is no change in the FWHM and fluorescence lifetime over time after the first injection of the Zn and S shelling precursors. However there is a small continuation of the λ_{max} blue-shift and increase of the QY and radiative rate over time after the large increase that occurred during the Zn and S shelling precursor injection. This is consistent with the formation of a ZnS shell. The surface passivation that a ZnS shell provides causes a decrease in surface trap states leading to the increase in the QY and radiative rate.[41,42] This, along with the structural analysis of no change in the size of the QDs and significant increase in the Zn composition, ~27%, leads to the conclusion that the ZnS shell was added by cation-exchange rather than by growth onto the core. This is also supported by the blue-shift in the λ_{max}, CIS is a Type I QD, meaning that the electron and the hole pair are confined in the core. If cation-exchange occurs to form the ZnS shell and the size of the QD not changing, this naturally means that the core of the QD is getting smaller.[43] Another cause for the blue-shift is the change in Cu:In ratio. Higher In compositions leads to a slow blue-shift, as has been observed previpously.[11] The first shelling injection leads to mainly cation-exchange between Cu and Zn, leaving Cu ions in solution, although a smaller amount In is also replaced. Another reason for large increase in the QY is that the formation of the ZnS-rich surface could lead to a stronger binding of the DDT and thus an additional route to surface trap passivation.[44, 22, 45, 4]

As the shelling temperature is lowered to 190°C or 170°C, the first injection of Zn and S led to a similar increase in Zn as at 210°C within the first hour but, in contrast to 210°C, reduced during the next 30 minutes (**Figure 3.13**). Interestingly, the reduction in Zn after 90 minutes at 190°C or 170°C did not lead to a reduction in the QY; in fact it continued to increase slightly. The QY increase is the result of the increase in the average radiative rate, k_r, with very little change in the average non-radiative rate, k_{nr}. This is basically the same trend observed at 210°C, albeit with the magnitude of the change decreasing with

temperature. Clearly the elimination of some Zn from the QD after 90 minutes does not lead to a reversing of the optical properties; it only slows down their change. It is likely that, at prolonged times, the Zn composition inside the QD is reduced but that the surface composition of Zn increases. In other words, the core and the shell are phase separating at lower temperature due to lattice self-purification of the CIS, but this competes with the dissolution of Zn from the particle, and the re-deposition of Cu and In from the solution. The same general trend in the changes during the first injection at 150°C or lower, but with a lower magnitude of change, suggest that this mechanism holds at lower temperatures. These results have shown that the lattice self-purification of CIS to remove Zn to the surface can be halted by increasing the temperature to between 190°C-210°C. This is an important result, since many reports of CIS/ZnS shelling fall within this temperature range, with some reports being closer to 190°C and others being closer to 210°C. [2, 46, 39, 40] This may explain why there are differences in some of their reported properties.

3.2.2 Second Injection

Whereas the first injection showed the same general trend in the QDs' optical properties for all shelling temperatures, the second injection of the Zn and S shelling precursors showed results that varied strongly with temperature. The major difference again occurred between the important 190°C and 210°C range. At 210°C, the QY significantly decreased and remained low, although the QD size and the Zn concentration in the QDs remained at the same level. Interestingly, at this temperature, the second injection correlated with an increase in the Cu concentration and a decrease in In in the QD. The Cu that had been "etched" away into the solution after the first injection then ion-exchanges with In at the QD surface forming new surface trap states;[47] the effect of increasing the Cu:In ratio on lowering the QY has been seen in other studies.[47, 48] It is unclear, however, why the addition of more Zn and S precursors leads to the Cu re-depositing in the QD. Perhaps it requires the formation of small Cu_2S clusters in order to do so, although this will be very difficult to prove. One argument supporting this assumption is that the ratio of Cu:In in all particles (even core-only CIS) is not 1:1, which suggests that the surface must be largely Cu_2S to obtain such ion ratios. This suggest an already core/shell architecture of CIS/Cu_2S in the as-synthesized CIS, which probably transitions into a CIS/$Cu_{2(1-x)}Zn_xS$ core/shell architecture after adding

Zn. The slow decrease in the λ_{max} and FWHM suggests a decrease in the number of low energy emission centers.[2] This loss of low energy emission centers could be the result of surface restructuring resulting from the Cu:In ratio increase leading to an increase in the non-radiative recombination at the surface.[6, 11] This conclusion is supported by the strong increase in the average non-radiative rate, k_{nr}, and the strong decrease in the average radiative rate, $k_{r,}$ (**Figure 3.10**).

At 190°C, the second injection initially caused a small decrease in the QY, but then rose over the next 1.5 hours to provide QDs with the highest QY. Most surprisingly, this correlated with complete exchange of Zn (and some In) with Cu. A similar behavior is observed at 170°C and lower, although the effect is very much reduced. If our proposed mechanism is correct, this reverts the CIS/$Cu_{2(1-x)}Zn_xS$ core/shell architecture formed after the first injection to a restructured CIS/Cu_2S core/shell architecture after the second injection in which QY is higher than if no Zn was added. In effect, the Zn is acting as a catalyst for QD restructuring at temperatures of 190°C or lower. The blue-shift in the λ_{max} but the increase in the FWHM for the second injection at 190°C or lower suggest that the size of the core may decrease, due to a thicker Cu_2S shell, but that the number of emission centers increases.[2] Again, this is consistent with the increase in the radiative rate, k_r, following the second injection at 190°C or lower, with lower temperatures having less of an effect.

3.2.3 Bi-temperature Shelling

Since a temperature of 210°C resulted in the highest QY after the first injection, but the second injection caused the QY to increase at temperatures of 190°C or lower, we hypothesized that bi-temperature shelling could yield even higher QY QDs. This was true, although the difference in QY between 210°C/190°C and double injection shelling at 190°C was not very significant. Using a low 90°C second injection temperature following the high 210°C first injection temperature yielded results that were basically the same as obtained from a single 210°C shelling injection, with the exception that the blue-shift and the FWHM decrease were halted by lowering the temperature. Clearly, the distribution of emission centers in the CIS/ZnS QD that affect the radiative and non-radiative rates that underlies the obtained QY in a kinetic process that can be tuned by both temperature and time. It may be possible to fine-tune the bi-temperature shelling more in order to obtain even higher QYs and correlate them to the

changing composition, but it is not expected that the results will be significantly improved. It is more likely that altering the Cu:In ratio in the initial CIS synthesis is a better route to increase the QY of the resulting CIS/ZnS QDs, since the composition ratio of the initial CIS followed by the number of injections and injection temperature will likely affect the ion-exchange reactions and the QD restructuring that is facilitated by lattice self-purification processes.

Chapter 4: Conclusions, Outlook, and Future Directions

4.1 Conclusions

The mechanism for CIS/ZnS shelling is proving to be quite different than binary II-IV QDs, such as CdSe. Instead of growing a shell onto the cores, whereby the QD size increases, it is produced via an ion-exchange reaction in which Zn replaces Cu and In, thereby keeping the QD small. In fact, the excess Cu compared to In in the QD suggest that as-synthesized CIS QDs already consists of a core/shell architecture of possibly CIS/Cu_2S. Adding Zn via this ion-exchange mechanism still leads to an increase in their QY, primarily by increasing the average radiative rate, k_r, by removing surface defects during shelling. The Zn concentration in the QD is maintained if the temperature is 210°C, probably by allowing the core and shell to anneal to some extent to reduce lattice strain. However, if the shelling temperature is 190°C or lower, the Zn starts to be removed from the QD over 1-2 hours due to lattice self-purification of CIS. Interestingly, the QY does not decrease during this restructuring process, although it is not as high as shelling with a single injection at 210°C where the Zn concentration is maintained.

Adding extra Zn and S precursors via a second injection at 190°C or lower leads to the Zn concentration dropping even further by re-exchanging the Zn in the QD with Cu. However, this reversing of the exchange does not lead to a decrease in the QY. In fact, with time, it can lead to an even higher QY than a single injection at 210°C. This is probably a result of surface restructuring of the QD catalyzed by the Zn. On the other hand, a second injection of Zn and S at 210°C leads to a significant decrease in the QY. The blue-shift in the emission and the decrease in the FWHM associated with this QY decrease suggests that this is a result of removing low-energy emission centers and replacing them with non-radiative processes that leads to an increase in k_{nr} and a decrease in k_r.

These results are important since most recent reports of CIS/ZnS synthesis have varied within the 190°C-210°C range and have had different shelling times.[40, 46, 39, 2] The kinetic effects of the ion-exchange reactions and lattice self-purification of CIS suggest that reaction time and temperature between 190°C and 210°C plays extremely important roles, and may explain the difference reported in CIS/ZnS optical and structural properties in the literature.

4.2 Outlook and Future Directions

The outlook for the use of CIS/ZnS in LEDs and fluorescent bioimaging applications using this new data is good because we have found that we can significantly increase the QY by carefully tuning reaction time and temperature. Moreover, it may be possible to further optimize the QDs' shelling and increase QYs even more without increasing their size. With further structural studies, in combination with spectroscopy, we hope to learn how we can decreasing the trap states and tune the number of emission centers to maintain a higher luminous efficiencies, longer fluorescence lifetimes and have even more control over the λ_{max} of the emission. One possible route for this it change the Cu:In ratio in the original CIS QDs[12] to tune the ion-exchange processes that lead to better core/shell architecture for increasing emission QY.

Other application can also be considered for future work. Since the QDs remain very small, there is the possibility of using them in drug delivery inside cells if they can be attached to a targeting moiety to the cells, where they can be internalized into the cell and release their drug cargo. Their small size will allow them to diffuse more deeply through tissue to reach that other targeting nanoparticles cannot. Since there is little to no toxicity compared to Cd-containing QDs, there is also not as much of a need to eliminate them from the organism rapidly. With their long fluorescence lifetimes, they can be used in advanced *in-vivo* imaging, such as time gated imaging to remove the cellular autofluorescence, increasing imaging sensitivity and allowing even lower concentrations to be used.

As mentioned previously, shelling CIS has proven very different than Cd-based QDs, which can lead to many different directions in terms of research. The structural properties still need to be further analyzed in order to completely understand the shelling and lattice self-purification mechanisms. The next step should be looking further into the crystal lattice structures of the QDs to see how the incorporation and then disappearance of the ZnS in the shell affects them. Also how the lattice mismatch is affected when the ZnS is still present in the shell after a second injection at 210°C should be studied to see why it has such a negative effect on the optical properties.

An important optical property that should be further investigated is the blinking mechanism. Since the shelling mechanism is so different in CIS than Cd-based QDs, one might expect the blinking behavior to be different upon shelling compared to the Cd-based QDs. Two main questions arise: Is the source of

the blinking the same as in Cd-based QDs or not? Is it possible to reduce the blinking in CIS QDs easier than for Cd-based QDs?

Finally, these experiments should also be repeated for shell materials other than ZnS. Possibly candidates include ZnSe and ZnTe incorporating other anions rather than S into the lattice may change the ion-exchange reaction that may allow the QY, λ_{max}, FWHM, k_r and k_{nr} to be tuned over a wider range. Ideally we would like to reach high QY, low FWHM, highly tunable λ_{max} from the UV up to the near infrared range, with fluorescence lifetimes in the several hundred nanoseconds range.

References

1. Petryayeva, E.; Algar, W. R., Quantum Dots in Bioanalysis: A Review of Applications Across Various Platforms for Fluorescence Spectroscopy and Imaging. *Applied Spectroscopy* 2012; Vol. 67, pp 215-252.

2. Shi, A.; Wang, X.; Meng, X.; Liu, X.; Li, H.; Zhao, J., Temperature-dependent photoluminescence of CuInS2 quantum dots. *J. Lumin.* **2012,** *132* (7), 1819-1823.

3. Stoneham, A. M.; Harker, A. H., Self-consistent calculations for shallow defects in semiconductors. II. Donor-acceptor pairs. *J. Phys. C* **1975,** *8* (8), 1109-18.

4. Omogo, B.; Aldana, J. F.; Heyes, C. D., Radiative and Nonradiative Lifetime Engineering of Quantum Dots in Multiple Solvents by Surface Atom Stoichiometry and Ligands. *J. Phys. Chem. C* **2013,** *117* (5), 2317-2327.

5. Hollingsworth, J. A., Heterostructuring Nanocrystal Quantum Dots Toward Intentional Suppression of Blinking and Auger Recombination. *Chem. Mater.* **2013,** *25* (8), 1318-1331.

6. Liu, L.; Hu, R.; Law, W.-C.; Roy, I.; Zhu, J.; Ye, L.; Hu, S.; Zhang, X.; Yong, K.-T., Optimizing the synthesis of red- and near-infrared CuInS2 and AgInS2 semiconductor nanocrystals for bioimaging. *Analyst (Cambridge, U. K.)* **2013,** *138* (20), 6144-6153.

7. Yoffe, A. D., Semiconductor quantum dots and related systems: electronic, optical, luminescence, and related properties of low-dimensional systems. *Adv. Phys.* **2001,** *50* (1), 1-208.

8. Schwartz, O.; Oron, D., A Present Understanding of Colloidal Quantum Dot Blinking. *Isr. J. Chem.* **2012,** *52* (11-12), 992-1001.

9. Ghaderi, S.; Ramesh, B.; Seifalian, A. M., Fluorescence nanoparticles "quantum dots" as drug delivery system and their toxicity: a review. *J. Drug Targeting* **2011,** *19* (7), 475-486.

10. Chen, C. W.; Wu, D. Y.; Chan, Y. C.; Lin, C. C.; Chung, P. H.; Hsiao, M.; Liu, R. S., Evaluations of the Chemical Stability and Cytotoxicity of CuInS2 and CuInS2/ZnS Core/Shell Quantum Dots. *Journal of Physical Chemistry C* **2015,** *119* (5), 2852-2860.

11. Chen, B.; Zhong, H.; Zhang, W.; Tan, Z.-a.; Li, Y.; Yu, C.; Zhai, T.; Bando, Y.; Yang, S.; Zou, B., Highly Emissive and Color-Tunable CuInS2-based Colloidal Semiconductor Nanocrystals: Off-Stoichiometry Effects and Improved Electroluminescence Performance. *Adv. Funct. Mater.* **2012,** *22* (10), 2081-2088.

12. Zhong, H.; Bai, Z.; Zou, B., Tuning the Luminescence Properties of Colloidal I-III-VI Semiconductor Nanocrystals for Optoelectronics and Biotechnology Applications. *J. Phys. Chem. Lett.* **2012,** *3* (21), 3167-3175.

13. Aldakov, D.; Lefrancois, A.; Reiss, P., Ternary and quaternary metal chalcogenide nanocrystals: synthesis, properties and applications. *J. Mater. Chem. C* **2013,** *1* (24), 3756-3776.

14. Van Sark, W. G. J. H. M.; Frederix, P. L. T. M.; Bol, A. A.; Gerritsen, H. C.; Meijerink, A., Blueing, bleaching, and blinking of single CdSe/ZnS quantum dots. *ChemPhysChem* **2002,** *3* (10), 871-879.

15. Song, W.-S.; Yang, H., Solvothermal preparation of yellow-emitting CuInS2/ZnS quantum dots and their application to white light-emitting diodes. *J. Nanosci. Nanotechnol.* **2013,** *13* (9), 6459-6462.

16. Xiong, W.-W.; Yang, G.-H.; Wu, X.-C.; Zhu, J.-J., Aqueous Synthesis of Color-Tunable CuInS2/ZnS Nanocrystals for the Detection of Human Interleukin 6. *ACS Appl. Mater. Interfaces* **2013,** *5* (16), 8210-8216.

17. Zhang, A.; Dong, C.; Liu, H.; Ren, J., Blinking Behavior of CdSe/CdS Quantum Dots Controlled by Alkylthiols as Surface Trap Modifiers. *J. Phys. Chem. C* **2013,** *117* (46), 24592-24600.

18. Deng, Z.; Schulz, O.; Lin, S.; Ding, B.; Liu, X.; Wei, X.; Ros, R.; Yan, H.; Liu, Y., Aqueous Synthesis of Zinc Blende CdTe/CdS Magic-Core/Thick-Shell Tetrahedral-Shaped Nanocrystals with Emission Tunable to Near-Infrared. *J. Am. Chem. Soc.* **2010,** *132* (16), 5592-5593.

19. Breus, V. V.; Heyes, C. D.; Nienhaus, G. U., Quenching of CdSe-ZnS Core-Shell Quantum Dot Luminescence by Water-Soluble Thiolated Ligands. *J. Phys. Chem. C* **2007,** *111* (50), 18589-18594.

20. Zhang, W.; Zhong, X., Facile Synthesis of ZnS-CuInS2-Alloyed Nanocrystals for a Color-Tunable Fluorchrome and Photocatalyst. *Inorg. Chem.* **2011,** *50* (9), 4065-4072.

21. Uehara, M.; Watanabe, K.; Tajiri, Y.; Nakamura, H.; Maeda, H., Synthesis of CuInS2 fluorescent nanocrystals and enhancement of fluorescence by controlling crystal defect. *J. Chem. Phys.* **2008,** *129* (13), 134709/1-134709/6.

22. Wuister, S. F.; Swart, I.; van Driel, F.; Hickey, S. G.; de Mello Donega, C., Highly Luminescent Water-Soluble CdTe Quantum Dots. *Nano Lett.* **2003,** *3* (4), 503-507.

23. Zhong, H.; Lo, S. S.; Mirkovic, T.; Li, Y.; Ding, Y.; Li, Y.; Scholes, G. D., Noninjection Gram-Scale Synthesis of Monodisperse Pyramidal CuInS2 Nanocrystals and Their Size-Dependent Properties. *ACS Nano* **2010,** *4* (9), 5253-5262.

24. Pan, D.; Weng, D.; Wang, X.; Xiao, Q.; Chen, W.; Xu, C.; Yang, Z.; Lu, Y., Alloyed semiconductor nanocrystals with broad tunable band gaps. *Chem. Commun. (Cambridge, U. K.)* **2009,** (28), 4221-4223.

25. Veilleux, V.; Lachance-Quirion, D.; Dore, K.; Landry, D. B.; Charette, P. G.; Allen, C. N., Strain-induced effects in colloidal quantum dots: lifetime measurements and blinking statistics. *Nanotechnology* **2010,** *21* (13), 134024/1-134024/6.

26. Durisic, N.; Wiseman, P. W.; Grutter, P.; Heyes, C. D., A Common Mechanism Underlies the Dark Fraction Formation and Fluorescence Blinking of Quantum Dots. *ACS Nano* **2009,** *3* (5), 1167-1175.

27. Durisic, N.; Godin, A. G.; Walters, D.; Grutter, P.; Wiseman, P. W.; Heyes, C. D., Probing the "Dark" Fraction of Core-Shell Quantum Dots by Ensemble and Single Particle pH-Dependent Spectroscopy. *ACS Nano* **2011,** *5* (11), 9062-9073.

28. Jorge, P.; Martins, M. A.; Trindade, T.; Santos, J. L.; Farahi, F., Optical fiber sensing using quantum dots. *Sensors* **2007,** *7* (12), 3489-3534.

29. Katari, J. E. B.; Colvin, V. L.; Alivisatos, A. P., X-ray Photoelectron Spectroscopy of CdSe Nanocrystals with Applications to Studies of the Nanocrystal Surface. *J. Phys. Chem.* **1994,** *98* (15), 4109-17.

30. Demir, H. V.; Nizamoglu, S.; Erdem, T.; Mutlugun, E.; Gaponik, N.; Eychmueller, A., Quantum dot integrated LEDs using photonic and excitonic color conversion. *Nano Today* **2011,** *6* (6), 632-647.

31. Aboulaich, A.; Michalska, M.; Schneider, R.; Potdevin, A.; Deschamps, J.; Deloncle, R.; Chadeyron, G.; Mahiou, R., Ce-Doped YAG Nanophosphor and Red Emitting CuInS2/ZnS Core/Shell Quantum Dots for Warm White Light-Emitting Diode with High Color Rendering Index. *ACS Appl. Mater. Interfaces* **2014,** *6* (1), 252-258.

32. Wang, H.; Shao, Z.; Chen, B.; Zhang, T.; Wang, F.; Zhong, H., Transparent, flexible and luminescent composite films by incorporating CuInS2 based quantum dots into a cyanoethyl cellulose matrix. *RSC Adv.* **2012,** *2* (7), 2675-2677.

33. Wijesundera, R. P.; Siripala, W., Preparation of CuInS2 thin films by electrodeposition and sulphurisation for applications in solar cells. *Sol. Energy Mater. Sol. Cells* **2004,** *81* (2), 147-154.

34. Chang, J.-Y.; Su, L.-F.; Li, C.-H.; Chang, C.-C.; Lin, J.-M., Efficient "green" quantum dot-sensitized solar cells based on Cu2S-CuInS2-ZnSe architecture. *Chem. Commun. (Cambridge, U. K.)* **2012,** *48* (40), 4848-4850.

35. Mandal, G.; Darragh, M.; Wang, Y. A.; Heyes, C. D., Cadmium-free quantum dots as time-gated bioimaging probes in highly-autofluorescent human breast cancer cells. *Chem. Commun. (Cambridge, U. K.)* **2013,** *49* (6), 624-626.

36. Foda, M. F.; Huang, L.; Shao, F.; Han, H.-Y., Biocompatible and Highly Luminescent Near-Infrared CuInS2/ZnS Quantum Dots Embedded Silica Beads for Cancer Cell Imaging. *ACS Appl. Mater. Interfaces* **2014,** *6* (3), 2011-2017.

37. Speranskaya, E. S.; Beloglazova, N. V.; Abe, S.; Aubert, T.; Smet, P. F.; Poelman, D.; Goryacheva, I. Y.; De Saeger, S.; Hens, Z., Hydrophilic, Bright CuInS2 Quantum Dots as Cd-Free Fluorescent Labels in Quantitative Immunoassay. *Langmuir* **2014,** *30* (25), 7567-7575.

38. Ding, K.; Jing, L.; Liu, C.; Hou, Y.; Gao, M., Magnetically engineered Cd-free quantum dots as dual-modality probes for fluorescence/magnetic resonance imaging of tumors. *Biomaterials* **2014,** *35* (5), 1608-1617.

39. Li, L.; Pandey, A.; Werder, D. J.; Khanal, B. P.; Pietryga, J. M.; Klimov, V. I., Efficient synthesis of highly luminescent copper indium sulfide-based core/shell nanocrystals with surprisingly long-lived emission. *J. Am. Chem. Soc.* **2011,** *133* (5), 1176-1179.

40. Xie, R.; Rutherford, M.; Peng, X., Formation of High-Quality I-III-VI Semiconductor Nanocrystals by Tuning Relative Reactivity of Cationic Precursors. *J. Am. Chem. Soc.* **2009,** *131* (15), 5691-5697.

41. Dias, E. A.; Saari, J. I.; Tyagi, P.; Kambhampati, P., Improving Optical Gain Performance in Semiconductor Quantum Dots via Coupled Quantum Shells. *J. Phys. Chem. C* **2012,** *116* (9), 5407-5413.

42. Jones, M.; Lo, S. S.; Scholes, G. D., Signatures of Exciton Dynamics and Carrier Trapping in the Time-Resolved Photoluminescence of Colloidal CdSe Nanocrystals. *J. Phys. Chem. C* **2009,** *113* (43), 18632-18642.

43. Park, J.; Kim, S.-W., CuInS2/ZnS core/shell quantum dots by cation exchange and their blue-shifted photoluminescence. *J. Mater. Chem.* **2011**, *21* (11), 3745-3750.

44. Hamada, M.; Takenokoshi, N.; Matozaki, K.; Feng, Q.; Murase, N.; Wakida, S.-i.; Nakanishi, S.; Biju, V., In Situ Photochemical Surface Passivation of CdSe/ZnS Quantum Dots for Quantitative Light Emission and Enhanced Photocurrent Response in Solar Cells. *J. Phys. Chem. C* **2014,** *118* (4), 2178-2186.

45. Wuister, S. F.; De Donega, C.; Meijerink, A., Influence of thiol capping on the exciton luminescence and decay kinetics of CdTe and CdSe quantum dots. *J. Phys. Chem. B* **2004,** *108* (45), 17393-17397.

46. Li, L.; Daou, T. J.; Texier, I.; Kim Chi, T. T.; Liem, N. Q.; Reiss, P., Highly Luminescent CuInS2/ZnS Core/Shell Nanocrystals: Cadmium-Free Quantum Dots for In Vivo Imaging. *Chem. Mater.* **2009,** *21* (12), 2422-2429.

47. Booth, M.; Peel, R.; Partanen, R.; Hondow, N.; Vasilca, V.; Jeuken, L. J. C.; Critchley, K., Amphipol-encapsulated CuInS2/ZnS quantum dots with excellent colloidal stability. *RSC Adv.* **2013,** *3* (43), 20559-20566.

48. Zhang, J.; Sun, W.; Yin, L.; Miao, X.; Zhang, D., One-pot synthesis of hydrophilic CuInS2 and CuInS2-ZnS colloidal quantum dots. *J. Mater. Chem. C* **2014,** *2* (24), 4812-4817.